

Star cluster ecology IVa: Dissection of an open star cluster—photometry

Simon F. Portegies Zwart,^{1*} Stephen L. W. McMillan,² Piet Hut,³ Junichiro Makino,⁴

¹ *Department of Astronomy, Boston University, 725 Commonwealth Ave., Boston, MA 02215, USA*

² *Department of Physics, Drexel University, Philadelphia, PA 19104, USA*

³ *Institute for Advanced Study, Princeton, NJ 08540, USA*

⁴ *Department of Information Science and Graphics, College of Arts and Science, University of Tokyo, 3-8-1 Komaba, Meguro-ku, Tokyo 153, Japan*

Accepted 1993 December 11. Received 1993 March 17

Key words: binaries: close — blue stragglers — stars: evolution — stars: mass loss — star clusters: general — star clusters: Pleiades, Hyades, Praesepe

ABSTRACT

The evolution of star clusters is studied using N -body simulations in which the evolution of single stars and binaries are taken self-consistently into account. Initial conditions are chosen to represent relatively young Galactic open clusters, such as the Pleiades, Praesepe and the Hyades. The calculations include a realistic mass function, primordial binaries and the external potential of the parent Galaxy.

Our model clusters are generally significantly flattened in the Galactic tidal field, and dissolve before deep core collapse occurs. The binary fraction decreases initially due to the destruction of soft binaries, but increases later because lower mass single stars escape more easily than the more massive binaries. At late times, the cluster core is quite rich in giants and white dwarfs. There is no evidence for preferential evaporation of old white dwarfs, on the contrary the formed white dwarfs are likely to remain in the cluster. Stars tend to escape from the cluster through the first and second Lagrange points, in the direction of and away from the Galactic center.

Mass segregation manifests itself in our models well within an initial relaxation time. As expected, giants and white dwarfs are much more strongly affected by mass segregation than main-sequence stars. However, the clusters to which we compare our results all appear to be somewhat more affected by mass segregation than our models would suggest.

Open clusters are dynamically rather inactive. However, the combined effect of stellar mass loss and evaporation of stars from the cluster potential drives its dissolution on a much shorter timescale than if these effects are neglected. The often-used argument that a star cluster is barely older than its relaxation time and therefore cannot be dynamically evolved is clearly in error for the majority of star clusters.

An observation of a blue straggler in an eccentric orbit around an unevolved star or a blue straggler of more than twice the turn off mass might indicate past dynamical activity. We find two distinct populations of blue stragglers: those formed above the main-sequence turn off, and those which appear as blue stragglers as the cluster's turnoff drops below the mass of the rejuvenated star.

1 INTRODUCTION

Star clusters are remarkable laboratories for the study of fundamental astrophysical processes spanning the range of

arXiv:astro-ph/0005248v1 11 May 2000

stellar evolution, from birth to death. Open clusters are relatively small (typically $\lesssim 10^4$ stars), young (generally $\lesssim 1$ Gyr old) systems found primarily in the Galactic disk. Roughly 1100 are known to lie within a few kiloparsecs of the Sun (Lynga 1987a). As a class, they afford us the opportunity to witness star formation and explore the complex evolution of young stellar systems. Since stars are born in star clusters and become part of the general Galactic population only when the parent cluster dissolves in the Galactic tidal field, it is of considerable interest to understand how this process occurs, on what time scale it operates, and what are the detailed observable consequences of cluster evolution.

At least as a first approximation, many star clusters are quite well characterized dynamically as pure N -body systems, in that there are few collisions or close encounters between stars and the clusters themselves are relatively isolated in space. The same argument can be made for the evolution of the stars and binaries without interactions, which may also quite well explain the properties of open clusters. This simple picture rapidly becomes inadequate when both effects are combined—cluster evolution is actually an intricate mix of dynamics, stellar evolution, and external (tidal) influences, and the subtle interplay between stellar dynamics and stellar physics makes for a formidable modeling problem. Of the many physical processes influencing cluster evolution, probably the most important are the effects of stellar evolution, the tidal field of the Galaxy, and the evolution and dynamics of binary stars. We present here a series of models in which all these effects are taken self-consistently into account.

The processes just mentioned are tightly coupled, complicating the evolution and making it difficult to isolate the importance of each individual effect. We refer to Meylan & Heggie (1997) for a recent review. Generally, speaking, we can say mass loss from stellar evolution is of greatest importance during the first few tens of millions of years of cluster evolution, and may well result in the disruption of the entire cluster (cf. Chernoff & Weinberg 1990, Fukushige & Heggie 1995, Takahashi & Portegies Zwart 2000). If the cluster survives this early phase, stellar evolutionary time scales soon become longer than the time scales for dynamical evolution, and two-body relaxation and tidal effects become dominant. Ultimately, these effects cause the cluster to dissociate and the stars to become part of the general “field” population of the disk.

There is strong observational evidence that star clusters contain substantial binary populations, quite possibly as rich as those found in the field (see Rubenstein 1997). The properties and numbers of observed cluster binaries cannot be explained by internal formation processes, such as three body dynamics or two body tidal capture (Aarseth & Lecar 1975). The majority must be primordial, i.e. formed together with the single stars at the cluster’s birth. These observations are important to cluster dynamics, as a cluster’s evolution depends strongly on its binary population and even a small initial binary fraction can play a pivotal role in governing cluster dynamics (Goodman & Hut 1989,

McMillan et al. 1990, 1991a and 1991b Gao et al. 1991, Hut et al. 1992, McMillan & Hut 1994). Binaries are also crucial to cluster stellar evolution. The possibility of mass transfer between binary components permits wholly new stellar evolutionary states to arise; in addition, the presence of binaries will enhance the rate of stellar collisions and close encounters, through the temporary capture of single stars and other binaries in three-body resonance encounters (Verbunt & Hut 1987; Portegies Zwart et al. 1998).

Until quite recently, dynamical models have tended to exclude binaries, for the good practical reasons that (1) binaries slow down the calculations dramatically and tend to induce numerical errors, and (2) their internal evolution is much more complicated than the evolution of single stars. However, it has also long been known that cluster models lacking adequate treatments of binary systems are of at best limited validity. In this paper we begin to address these limitations by performing calculations of open clusters containing substantial numbers of primordial binaries, with the goal of studying the mutual influence of stellar evolution and stellar dynamics in these systems—the “ecology” of star clusters (Heggie 1992).

The first paper in this series (Portegies Zwart et al. 1997a, hereafter paper I) quantified the effect of collisions on stellar evolution and attempted to assess the corresponding changes in the stellar population. The stellar number density was held constant in these calculations, thus excluding the possibility of any interplay between the dynamical evolution of the cluster and collisions between stars. In the second paper in this series (Portegies Zwart et al. 1997b, hereafter paper II), the evolution of a population of primordial binaries was followed in time by tracking in detail the results of encounters between single stars and binaries. The assumption of constant stellar number density was relaxed in Portegies Zwart et al. (1999, hereafter paper III), where the dynamical evolution of a star cluster (without primordial binaries) was followed in detail using N -body calculations.

This paper continues the process of relaxing the simplifying assumptions made in Paper I. As in Paper III, we calculate the dynamical evolution of our model system by direct (N -body) integration of the system, but now including both stars and binaries in the computational mix. Binary evolution is incorporated into the N -body treatment, accounting for changes in binary orbital parameters due to stellar mass loss, supernovae, tidal forces between the stars, mass transfer from one star to its companion, general relativistic corrections, etc. Encounters between binaries and single stars and higher order encounters (between binaries and binaries and between binaries and triples etc.) are fully integrated as are the orbits of the other stars in the N -body system. All changes in the stellar and binary population caused by stellar evolution are fed back into the dynamical evolution of the parent cluster, allowing stellar dynamics and the stellar evolution to be studied simultaneously and self-consistently.

As an initial case study, we concentrate here on open star clusters near the Sun (between ~ 6 and 10 kpc from the Galactic center), which are less than 1 billion years old, and

which initially contain a few thousand (~ 2000 – 3000) stars, roughly half of them in binaries. Well known clusters fitting this general description are the Pleiades, Praesepe and the Hyades. Such systems are small enough that multiple simulations can be performed in order to improve statistical coverage of their properties, yet they are large enough and old enough that both stellar evolution and stellar dynamics have had time to play significant roles in determining their present structure and appearance.

In an effort to close the gap between theoretical and observational studies of cluster structure, in this and subsequent papers we will attempt wherever possible to “observe” our model clusters using techniques similar to those employed by observers. For this paper we have chosen to adopt a “photometric” approach. Consequently, we present little detailed information about the binaries in our calculations. Binary properties will be discussed in depth in a “spectroscopic” companion paper (Portegies Zwart et. al, Paper IVb, in preparation).

Section 2 discusses the choice of initial conditions and parameters for our model clusters. The results of the calculations are presented in §3, followed in section 4, which compares our results with selected observations on a cluster-by-cluster basis. Section 5 our results with some previous studies in this area. We summarize in §6. Two appendices are included, Appendix A gives an overview of the terminology used throughout the paper; Appendix B reviews the “Starlab” software package and the implementation and coupling of its two main constituents kira (the N -body integrator §B1) and SeBa (the stellar/binary evolution program §B2).

2 INITIAL CONDITIONS

In order to begin a simulation, a number of critical cluster parameters must be chosen: the mass, virial radius, and tidal radius (or its equivalent), the initial mass function, and the initial distributions of binary spatial density and orbital properties. Table 1 presents an overview of observed parameters for some star clusters with similar overall masses, stellar membership and half-mass radii. The ages of these clusters vary widely, from about 110 Myr (Pleiades) to over 1 Gyr (NGC 3680). Their core and half mass radii suggest that they may be described approximately by King models (King 1966) with dimensionless depths in the range $W_0 \sim 4 - 6$, where larger W_0 corresponds to higher central concentration.

We define our mass scale by arbitrarily adopting a “Hyades-like” model, in which the mass of the system at an age of 625 Myr is $\sim 1000M_\odot$. We then estimate the initial mass of a cluster by applying a number of corrections. We adopt the initial mass function for the solar neighborhood described by Scalo (1986). Table 2 shows how the Scalo mass function evolves in time. Approximately 20% of the initial mass is lost by purely stellar-evolutionary processes. (Binary evolution complicates matters which we neglect in these rough numbers.)

Table 2. Number N_x of stars of type x and total mass M , from the Scalo (1986) initial mass function, evolved with SeBa. Calculation was performed with a population of 100k stars, but the numbers are normalized to 1k stars.

time [Myr]	0	100	200	400	600	800
ms	1024	1014.7	1007.7	996.7	988.3	982.1
gs	0	2.7	4.3	6.2	6.2	5.8
wd	0	3.0	8.5	17.6	26.0	32.7
ns	0	3.6	3.6	3.6	3.6	3.6
$M [M_\odot]$	624.4	562.3	541.5	517.6	501.1	490.6

In addition to stellar evolution, dynamical evolution of the star cluster and the tidal field of the Galaxy also tend to consume (eject) cluster stars, at a rate of about 10% per relaxation time (Spitzer 1987). With a current relaxation time for Hyades of about 400Myr (see Table 1) we estimate that the amount of mass lost by dynamical processes up to an age of 625 Myr is similar to the mass lost to stellar evolution. Adding these numbers provides a conservative lower limit to the amount of mass lost by the star cluster. This limit is conservative because we neglected the interaction between stellar mass loss and dynamical mass loss and the extra mass loss induced by interactions with giant molecular clouds. We therefore adopt an initial cluster mass of $M_0 \sim 1600 M_\odot$. This is close to the $1800 M_\odot$ for the initial mass of Hyades derived by Weidemann (1992). We assume a Scalo (1986) initial mass function, with minimum and maximum masses of $0.1 M_\odot$ and $100 M_\odot$, respectively, and mean mass $\langle m \rangle \simeq 0.6 M_\odot$. Consistent with the above estimates, our simulations are performed with 1024 single stars and 1024 binaries, for a total of 3096 (3k) stars and a binary fraction of 50%.

Stars and binaries within our model are initialized as follows. A total of 2k single stars are selected from the initial mass function and placed in an equilibrium configuration in the selected density distribution (see below). We then randomly select half the stars and add a second companion star to them. The masses of the companions are randomly selected between $0.1 M_\odot$ and the primary mass. For low-mass primaries, the mass ratio distribution peaks at unity, whereas the distribution is flat for more massive primaries. Once stellar masses are chosen, other binary parameters are determined. Binary eccentricities are selected from a thermal distribution between 0 and 1. Orbital separations a are selected with equal probability in $\log a$ with the lower limit set by the separation at which the primary fills its Roche lobe or at $1 R_\odot$, whichever is smaller. The upper limit for the initial semi-major axis is taken at $10^6 R_\odot$ (about 0.02 pc, Duquennoy & Mayor 1991). When a binary appears to be in contact at pericenter, new orbital parameters are selected. Table 3 gives an overview of the various distribution functions from which stars and binaries are initialized.

We select initial density profiles from the anisotropic density distributions described by Heggie & Ramamani

Table 1. Observed and derived parameters for several open star clusters with which our simulations may be compared. Subsequent columns give (3) the distance to the cluster (in pc), (4) the cluster age (in Myr), (5) the half mass relaxation time (in Myr), (6) the total mass (in M_{\odot}), (7) the tidal radius (in pc), (8) estimate for the half mass radius (in pc), and (9) the core radius (in pc). In cases where the parameters (relaxation time, mass, etc.) are not accessible in the literature, we calculate it; these entries are printed *in italics*. In most cases these numbers can be calculated using Eq. A9 or Eq. A10. Dashes and question marks indicate that we cannot derive these numbers from the literature. The final two columns contain information on the cluster stellar content. The column labeled $f_{s:b:t}$ indicates the number of single stars, binaries and triples (separated by colons). For clusters where the numbers are given directly by observations, the table gives the observed numbers of each system. If the binary fraction is derived by other methods, we give the relative fractions normalized to the number of single stars. The last column ($N_{\text{bss:gs:wd}}$) gives the number of observed blue stragglers, giants and white dwarfs, separated by colons.[‡]

name	ref.	d [pc]	t [Myr]	t_{rlx}	M [M_{\odot}]	r_{tide}	r_{hm} [pc]	r_{core}	$f_{s:b:t}$	$N_{\text{bss:gs:wd}}$
NGC 2516	a	373	110	<i>220</i>	<i>1000</i>	<i>13</i>	2.9	—	16:6:?	6:4:4
Pleiades	b	135	115	150	~ 1500	16	2–4	1.4	137:60:2	0:3:3
NGC 2287	c	655	160–200	—	$\gtrsim 120$	6.3	—	—	1:0.6:?	3:8:3
Praesepe	d	174	400–900	<i>370</i>	1160	12	<i>3.5</i>	2.8	1:0.3:0.03	5:5:11
Hyades	e	46	625	<i>390</i>	500–1000	10.3	<i>3.7</i>	2.6	1:0.4:0	1:4:10
NGC 2660	f	2884	900–1200	<i>315</i>	$\gtrsim 400$	<i>9.6</i>	4	<i>1.5</i>	1:0.3:?	18:39:?
NGC 3680	g	735	1450	<i>28</i>	$\gtrsim 100$	4.3	1.2	<i>0.6</i>	44:25:0	4:17:?

References to the literature (second column) are: (a) Abt & Levy (1972); Dachs, J & Kabus (1989); Hawley et al. (1999). (Note: we interpret the quoted limiting cluster radius as the half mass radius.) (b) Pinfield et al. (1998); Raboud & Mermilliod, (1998); Bouvier et al (1998); (c) Harris et al. (1993); Ianna et al (1987); Cox (1954). (d) Andrievsky (1998); Jones & Stauffer (1991); Mermilliod & Mayor (1999); Mermilliod et al. (1990); Hodgkin et al. (1999). (Note: we interpret the quoted central radius for the cluster as the half mass radius.) (e) Perryman et al. (1998 and references therein) Reid & Hawley (1999); (f) Frandsen et al. (1989); Hartwick & Hesser (1971); Sandrelli et al. (1999). (g) Hawley et al. 1999 ; Nordström et al. (1997); Nordström et al. (1996), Data on numbers of white dwarfs was taken from Anthony-Twarog (1984) for Praesepe, from Koester & Reimers (1987) for NGC 2287 and from von Hippel (1998) for the other clusters.

Table 3. Initial conditions for the stellar and binary population. The first column gives the parameter, the second and third columns give the symbol and the distribution function, followed by the lower and upper limits adopted.

parameter	function	limits	
		lower	upper
primary mass	M $P(M) = \text{Scalo (1986)}$	$0.1 M_{\odot}$	$100 M_{\odot}$
secondary mass	m $P(m) = \text{constant}$	$0.1 M_{\odot}$	M
orbital separation	a $P(a) = 1/a$	RLOF	$10^6 R_{\odot}$
eccentricity	e $P(e) = 2e$	0	1

(1995) with $W_0 = 4$ and $W_0 = 6$, and refer to these models as W4 and W6, respectively throughout this paper. The Heggie-Ramamani models are derived from King (1966) models, but take into account the velocity anisotropy and non-spherical shape of the critical zero-velocity (Jacobi) surface of the cluster in the Galactic tidal field. (The classical King models have spherical boundaries.) Within the half mass radius, the Heggie-Ramamani models are quite isotropic.

All models are started with a virial radius of $r_{\text{vir}} = 2.5$ pc. For our adopted parameters, the initial cluster dynamical time scale is then $t_{\text{hm}} \equiv (GM/r_{\text{vir}}^3)^{-1/2} \sim 1.5$ Myr. Each cluster is assumed to precisely fill its Jacobi surface at birth. (Expressed less precisely, we could say that the limiting ra-

dius of the initial King model is equal to the Roche radius of the cluster in the Galactic tidal field.) Given the Oort constants in the solar neighborhood, we find that the models with $W_0 = 6$ are somewhat farther (~ 12.1 kpc) from the Galactic center than is the Sun, while a model with $W_0 = 4$ is slightly closer (~ 6.3 kpc).

For a total cluster mass of $1600 M_{\odot}$, the Lagrange points of our two standard clusters lie, respectively, at 14.5 pc ($W_0 = 4$) and 21.6 pc ($W_0 = 6$) from the cluster center. A star is removed from a simulation when its distance from the cluster’s density center exceeds twice the distance from the center to the first Lagrangian point.

Table 4 reviews the adopted parameters and initial conditions of our models. In order to improve statistics, we performed four calculations (labeled I through IV) for each set of initial conditions. A fifth run is performed as a pioneering study for each set of initial conditions but they are terminated at 400 Myears.

3 RESULTS

We now discuss the “photometric” properties of our model clusters. As mentioned above, we defer the discussion of “spectroscopic” properties, including details on the various types of binaries found in our simulations, to Paper IVb.

Table 4. Initial conditions and parameters for the selected models. The columns give the model name, initial mass (M_{\odot}), number of stars, dimensionless central depth of the potential well (W_0), the distance from the Galactic center (kpc), the initial relaxation and half mass crossing times (both in Myr), r_x , r_y , and r_z , the distances from the cluster center to the Jacobi surface (so r_x is simply the Jacobi radius, r_J ; see Appendix A), and the virial, half mass and core radius (all in parsec).

name	M [M_{\odot}]	N	W_0	R_{Gal} [kpc]	t_{rlx} [Myr]	t_{hm} [Myr]	r_{Jacob}	r_{vir}	r_{hm}	r_{core}		
							[pc]	[pc]	[pc]			
W4	1600	3k	4	6.3	109	4.07	14.5	9.7	7.2	2.5	2.14	0.83
W6	1600	3k	6	12.1	102	4.15	21.6	14.4	10.8	2.5	2.00	0.59

Table 5. Overview of the variation in parameters for model W6-III. The realization of the initial mass function was identical for all these models. Other parameters are as in Tab. 4. For each of these calculations some feature of starlab was switched on (+) or off (-); kira (the N -body integrator), SeBa (the stellar and binary evolution model) and whether the calculation started with primordial binaries.

	Starlab		Primordial binaries
	kira	SeBa	
upper solid	-	+	+
lower solid	+	-	+
dashes	+	+	+
dash-dots	+	+	-

3.1 Global properties

Figure 1(a) shows the mass of the cluster as a function of time for several models. In this figure, the “total mass” of a model is simply taken to be the sum of the masses of all stars remaining within the N -body system. This overestimates both the bound mass of the system and probably also the mass that would be derived by observers, and therefore provides a firm upper limit to the “true” mass. The dashed line gives the results from model W6-III. The two dotted lines show the mass evolution of two of the W4 models (upper line: model W4-III, lower line: W4-IV), illustrating the run-to-run variations in dynamical evolution (which are mainly the result of an initial offset between the masses of the two models, caused by different random seeds).

Table 5 indicates the differences between the various line styles in Fig. 1(a). All lines listed are computed using exactly the same stellar masses as in model W6-III.

The two solid lines in Figure 1(a) show (upper line) the total mass of an N -body system without stellar evolution, but otherwise with the same initial conditions as run W6-III, and (lower line) the total mass of stars, excluding stellar dynamics but including mass loss by stellar evolution (with the same initial stellar masses as in model W6-III; see Table. 5 for an review of the line styles). Mass loss in the absence of stellar evolution is not linear with time, as one expects from a equal mass N -body system; the presence of a mass function causes heavier stars generally to be lost later, resulting in larger mass loss at later time. However, the loss rate of

stars is roughly constant, and the curvature of the upper solid line in Figure 1(a) demonstrates the strong effects of mass segregation and cluster dynamics.

The actual variation of the cluster mass (under the combined effects of stellar mass loss and dynamical evolution) is larger than the sum of the two separate effects by about a factor two. For the selected initial conditions, the interplay between stellar evolution and stellar dynamics is especially important during the later stages of the evolution. The presence of primordial binaries has little effect on the evaporation rate of the clusters. The dash-dotted line gives the total mass of the same model, but without binaries—all stars in the initial mass function (including binary secondaries) are redistributed with the same density profile as model W6-III. As noted by McMillan & Hut (1994), primordial binaries have little effect on the overall rate at which mass is lost from the cluster.

Figure 1(b) shows the masses of two model clusters (W6-III and W4-II), with different criteria for the limiting radius of the stellar system. The solid lines give the total mass in the N -body system (see also Figure 1[a]), the dotted lines the total mass within the Jacobi surface, and the dashed lines the total mass within the Jacobi radius of the cluster center, as seen by an observer looking along the y -axis. The total mass in stars in the N -body system overestimates the cluster’s mass; the mass within the zero velocity surface may give a better measure of the mass one would observe in a real situation. The cluster mass within the Jacobi radius, viewed along the x -axis, always lies between the solid and dotted lines; the corresponding mass viewed along the z axis lies between the dotted and the dashed lines. These trends are found in all models studied.

Figure 2(a) presents the observational equivalent of Figure 1(b), showing the total M_V magnitude of the W6 models at various times. The spread in M_V is caused by the intrinsic differences between runs—initial conditions, run-to-run variations and fluctuations due to the small numbers of giants, which dominate the total magnitude. Note that, for technical reasons, the output intervals are not the same for the four calculations shown here.

Figure 2(b) plots the integrated $B - V$ color of the cluster as a function of time. The initial color of all models is confined to a small range between $B - V \simeq -0.15$ and -0.28 , but rapidly grows to larger values with a larger spread: $B - V \simeq 0.1-0.4$ at 50 Myr and $B - V \simeq 0.5-0.8$

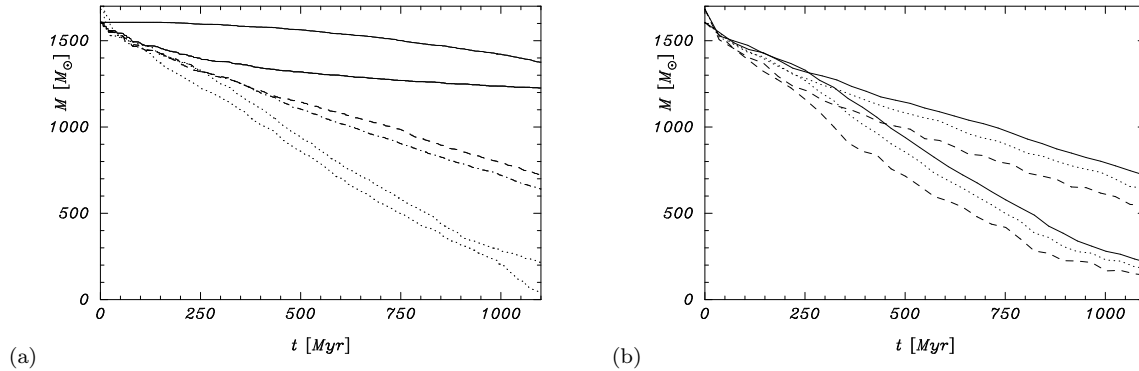


Figure 1. (a) Mass (in M_{\odot}) as a function of time (in Myr) for various models. The solid lines show the time-dependence of the total mass with (upper curve) stellar evolution suppressed, and (lower curve) without dynamical evolution. The dashed line is the total mass of model W6-III. The dot-dashed line is the total mass of a calculation with the identical mass function as in model W6-III, but all stars were single and redistributed in an identical density distribution. This line therefore gives the difference in a calculation with or without primordial binaries, but with all the other effects taken the same. The dotted lines represent the total mass of models W4-II (upper) and W4-IV (lower). (b) Various definitions of the cluster mass (in M_{\odot}) as functions of time for model W6-III (upper set of 3 lines) and model W4-II (lower set of lines). Solid lines represent the total mass in the N -body system, dotted lines the mass within the Jacobi surface, and dashed lines the total mass seen in projection within a distance r_J of the cluster center.

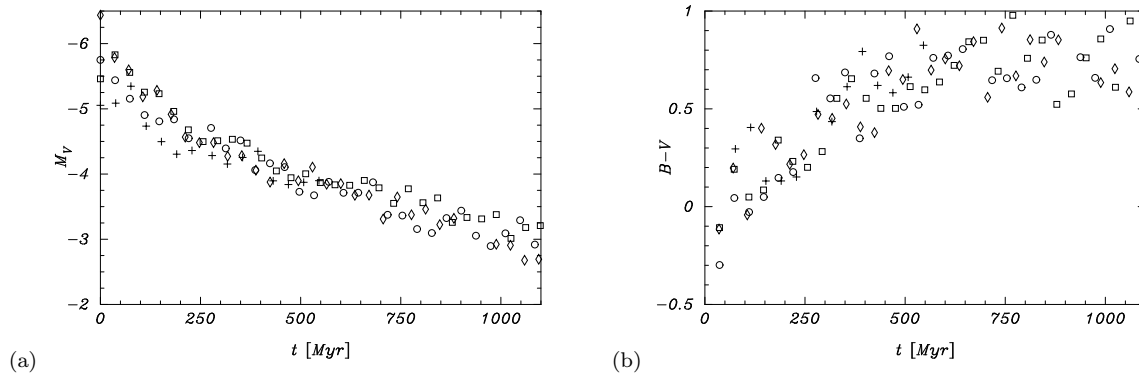


Figure 2. (a) Integrated M_V magnitude as a function of time of the four W6 models (plus, circle, square, and diamond give the data for the models I–IV). The variation between the points at similar times within a single calculation is comparable to the visible spread in the data. (b) Integrated $B - V$ color as a function of time for the W6 models.

at 500 Myr. As in Figure 2(a), the intrinsic spread is caused by the presence of a relatively small number of giant stars. The increase in the color index indicates that the cluster gets redder with age, which is mainly due to the loss of the massive blue stars and the formation of red giants. The color variation of the W4 models is similar.

Figures 3 shows how the radii of models W4 and W6 evolve with time. All stars in the N -body system are taken into account in calculating the Lagrangian radii. The outer radii therefore expand much more than they would do if only stars within the Jacobi surface were considered. Note the absence of any discernible core collapse in either case. There is a slight, barely noticeable, core contraction between

$t = 100$ and 150 Myr for the W6 models, and somewhat earlier for the W4 models, but neither is very deep. This shallow core contraction phase demonstrates the importance of stellar mass loss and, to a lesser extent, binary heating to the dynamical evolution of these systems; mass segregation for example, which also plays an important role here (see Fig. 5). A comparable model with primordial binaries and without stellar evolution would experience core collapse (McMillan et al. 1990, 1991), even in the presence of a Galactic tidal field (McMillan & Hut 1994).

In contrast to the W6 radii shown in Figure 3(a), the Lagrangian radii of model W4-II (Figure 3[b]) expand for about 300 Myr, and subsequently shrink. The decrease in

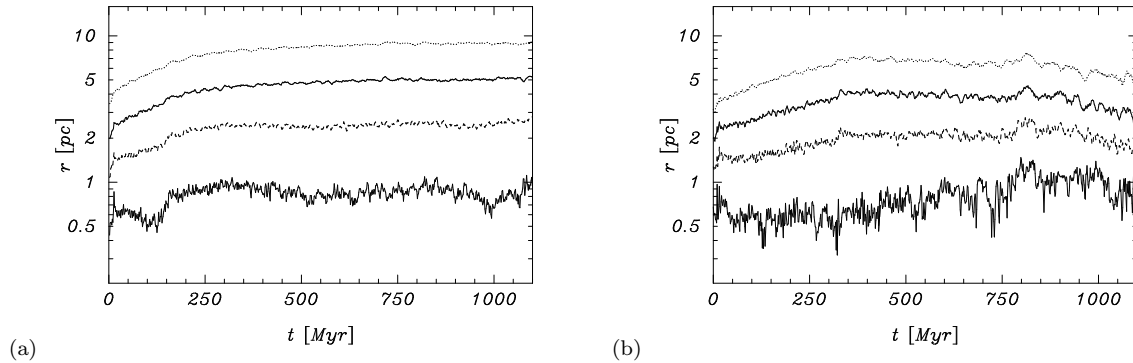


Figure 3. Lagrangian radii (in pc) as functions of time. The data in (a) represent the mean of the four W6 runs, those in (b) model W4-II. From top to bottom, the radii contain the following mass fractions: 75% (dots), 50% (upper solid), 25% (dashes) and 5% (lower solid).

Lagrangian radii at late times is an indicator of cluster evaporation. As the cluster dissolves in the Galactic tidal field, its tidal radius decreases, accelerating the dissolution and causing the Lagrangian radii to decrease. The W6 clusters show the same behavior, but at somewhat later times. We show the result of a single W4 model to illustrate the intrinsic fluctuations within a single N -body run.

Finally, Figure 4 shows the half-mass relaxation time (Eq. A9) as a function of time for models W6-III (solid line) and W4-II (dashed line). Note that the relaxation time peaks around the cluster’s “half-life” epoch—750 and 400 Myr for models W6-III and W4-II, respectively. Consequently, estimates of the present-day relaxation time of observed open clusters may provide poor indicators of the dynamical age of the stellar system. The often-used argument that a star cluster is barely older than its relaxation time and therefore cannot be dynamically evolved is clearly in error for the majority of star clusters (see also McMillan & Hut 1994).

3.2 Mass segregation

The effect of mass segregation is clearly visible in Figure 5(a), which shows the mean mass $\langle m \rangle$ of stars within the 5%, 25%, 50% and 75% Lagrangian radii as functions of time, averaged over the four W6 models. The initial increase in the mean mass within the inner 5% Lagrangian radius is the result of mass segregation. The value of $\langle m \rangle$ in the cluster center decreases again after about 100 Myr, when the most massive stars leave the mean sequence and lose most of their mass on the Asymptotic Giant Branch. For the remainder of the calculation $\langle m \rangle$ stays more or less constant in each Lagrangian zone, but with a significantly higher value in the inner zones.

Figure 5(b) shows the evolution of the mean mass $\langle m \rangle$, in model W4-II. Mass segregation in this model proceeds on a longer time scale than in the W6 models, but the cluster dissolves on a shorter timescale. Near the end of the cluster

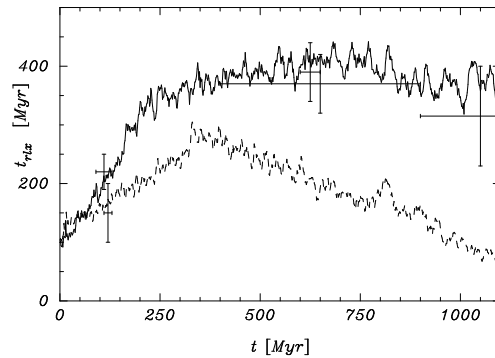


Figure 4. Half-mass relaxation time as a function of time for the models W6-III (solid) and for model W4-II (dashes). The error bars indicate the computed relaxation times for the observed star clusters from Table 1. (Confidence intervals are not listed in the table.)

lifetime the mean mass in the outer regions increase, caused by the preferential loss of the lower mass stars by evaporation. The more massive stars have greater difficulty to climb out of the potential well.

Figure 6 shows the mean mass to light ratio for the W6 models. Except for the first few million years, the mass-to-light ratio in the cluster core is always substantially smaller (and noisier) than that in the halo, as mass segregation causes the most massive (i.e. brightest) stars to sink rapidly to the cluster center. The general increase in mass-to-light ratio with time is the result of stellar evolution, the loss of lower-mass stars by tidal stripping compensates somewhat. The occasional dips in the mass-to-light ratio are caused by individual red giant stars; most of these dips occur in the core, where mass segregation causes the giants to accumu-

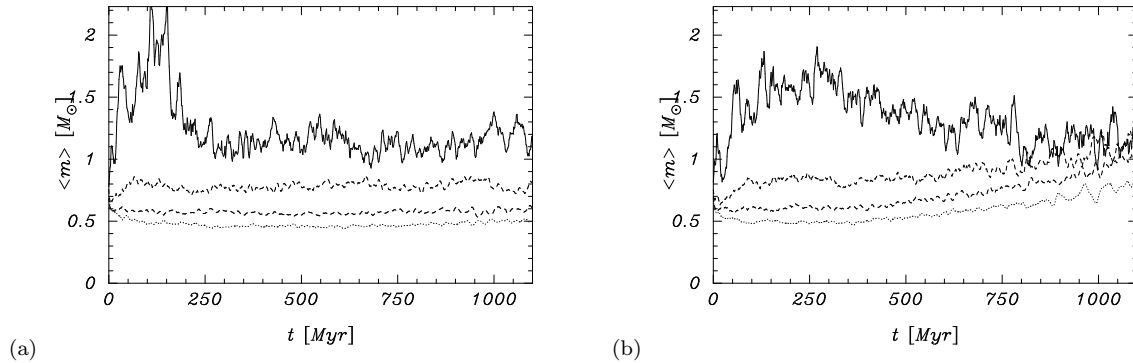


Figure 5. (a and b) The mean mass $\langle m \rangle$ of model W6-III (a) and W4-II (b), as functions of time. The data have been smoothed over time intervals of 8.8 Myr. From top to bottom, the lines represent the mean mass within the 5% (solid), 25% and 50% (dashes), and 75% (dots) Lagrangian radii (see Fig. 3 for the corresponding radii.)

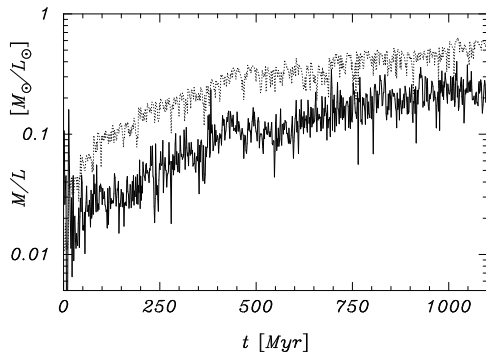


Figure 6. The mean mass to light ratio for models W6-I to IV, within the 5% (solid) and 75% (dots) Lagrangian radii.

late. We can reduce this “noise” considerably by averaging over the four W6 calculations, but the effect remains visible.

Figure 7(a) shows the radial stellar distribution in the W6 models at various epochs. The cluster expands as it ages. The binaries (dotted lines) closely follow the distribution of the single stars for the first 100 Myr, but become more centrally concentrated at later epochs. Mass segregation is also clearly visible if we compare the radial distributions of low mass (faint) stars with the more massive (bright) stars (Figure 7[b]). Stars with $L > 0.5 L_{\odot}$ are clearly more centrally concentrated than the mean cluster star, while giants (although there are only a few) are even more strongly concentrated in the cluster center.

Mass segregation can also be observed in the cluster’s mass and luminosity functions. Figure 8(a) shows global mass functions for all single stars and binary primaries for the W6 models at birth and at $t = 600$ Myr. The global mass function of the cluster is affected only slightly by stellar evo-

lution and mass segregation. However, the mass function at $t = 600$ Myr for stars in the inner part of the cluster (dot-dashed line) is clearly different from the global mass function at that time.

The white dwarfs are more centrally concentrated than stars with luminosity $> 0.5 L_{\odot}$ and slightly less concentrated than the giants (see Fig. 7[b]). This is caused by the progenitors of the white dwarfs, the giants, being centrally concentrated while after their envelopes are shed they have masses comparable to the the mean cluster stars. Segregating outwards takes more time than sinking inwards and at the same time more white dwarfs are produced in the cluster center (see the end of this section for more details).

Figure 8(b) shows the luminosity functions (in M_V) for stars (including binaries) in models W6 at zero age and at 600 Myr. Note that the luminosity function at the later time shows a *larger* fraction of bright stars. The reason is two fold: 1) stellar evolution has removed only the most massive stars by this time, while mass segregation has concentrated the remaining massive (bright) stars in the cluster core, at the same time causing the lower mass stars to escape and 2) heaviest stars turn into giants, which for older (lighter) stars are much brighter than main-sequence stars, whereas for younger (heavier) stars, the difference in brightness between giant and main-sequence star is much smaller.

The W4 models more strongly affected by mass segregation (not shows but see sect 4). In part, this is caused by the more rapid evaporation of these models compared to the W6 models. This is consistent with the findings of Takahashi & Portegies Zwart (2000), who noted that clusters which are close to complete disruption contain a higher fraction of high-mass stars.

3.3 Hertzsprung–Russel diagrams

Figure 9 shows a time sequence of Hertzsprung–Russel diagrams for model W6-III. The youngest Hertzsprung–Russel

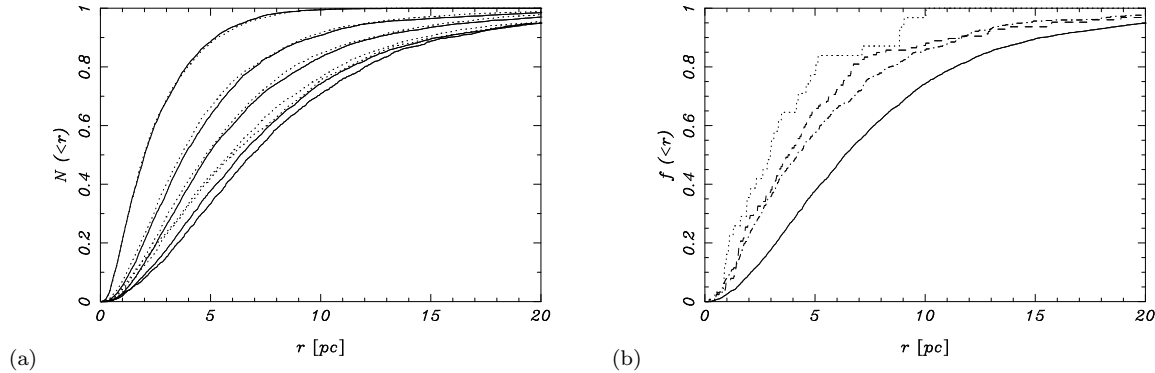


Figure 7. (a) Cumulative distribution of single stars (solid lines) and binaries (dotted lines), averaged over the four W6 models, at (upper left to lower right) $t = 0, 100, 200, 600,$ and 800 Myr. (b) Cumulative distribution of various stellar populations for the four W6 runs at an age of 600 Myr. Solid line: the distribution of all stars (see also the lower solid line in Figure 7[a]); dash-dotted line: stars with $L > 0.5L_{\odot}$; dashed line: white dwarfs; dotted line: (sub)giants.

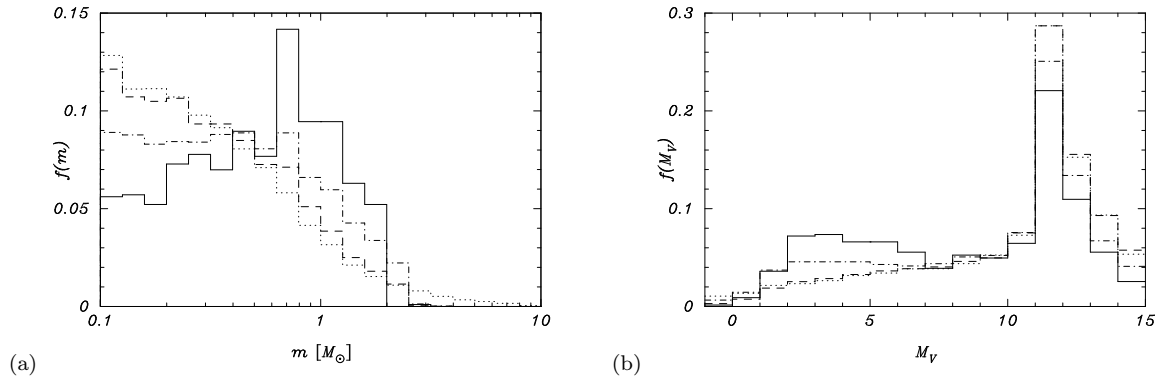


Figure 8. mass function (a) and luminosity function (b) for model W6. The dotted lines give the $t = 0$ distributions and the dashed lines give the distributions at $t = 600$ Myr (averaged over all models). The dash-dotted lines are the mass (luminosity) functions for stars within 3.4 pc (the half-mass radius for W6 models at $t = 600$ Myr) of the density center (for [b] in projection, as viewed along the x axis). The solid line gives the mass function of the W6 models within 3.4 pc (projected again for [b]) at an age of 1100 Myr.

diagram (200 Myr) already shows a white dwarf sequence. Note the densely populated “binary sequence” ~ 0.75 magnitudes above the zero-age main-sequence. One of the objects in the middle panel (close to but just above the turnoff) is a blue straggler; the other two are binaries (see also Figure 11). The objects immediately to the left of the main sequence (the two points in the 600 Myr diagram at $B - V \sim 1.18$ and the single point at $B - V \sim 0.5, V = 8$) are binaries containing a mass-transfer remnant (a helium star) and a main-sequence star which has accreted part of its companion’s envelope. Farther to the blue (between $B - V = 0$ and 0.8), but to the right of the white dwarf sequence, are binaries consisting of a white dwarf and a low-mass main-sequence star (several are seen in the 600 Myr and 1100 Myr diagrams). In the bottom panel a break and discontinuity in the zero-age main-sequence is visible near $B - V = 0.4$ and

at $V \simeq 4$. This is an artifact of the stellar evolution fitting formulae given by Eggleton, Fitchet & Tout (1989) and appears when the envelope of a main-sequence star becomes convective.

Figure 10 shows Hertzsprung–Russell diagrams for the inner, middle and outer regions of the combined W6 models at an age of about 600 Myr, and illustrates the effect of mass segregation. Each diagram contains about 2000 objects. The slight “fuzziness” near the main-sequence turnoff is the result of variations in output times between individual simulations, which cause the combined diagram to have a small spread in stellar ages. About one quarter (one run) of the stars come from a slightly younger cluster with an age of about 550 Myr.

The Hertzsprung–Russell diagrams of the inner and outer parts of the cluster show significant differences due

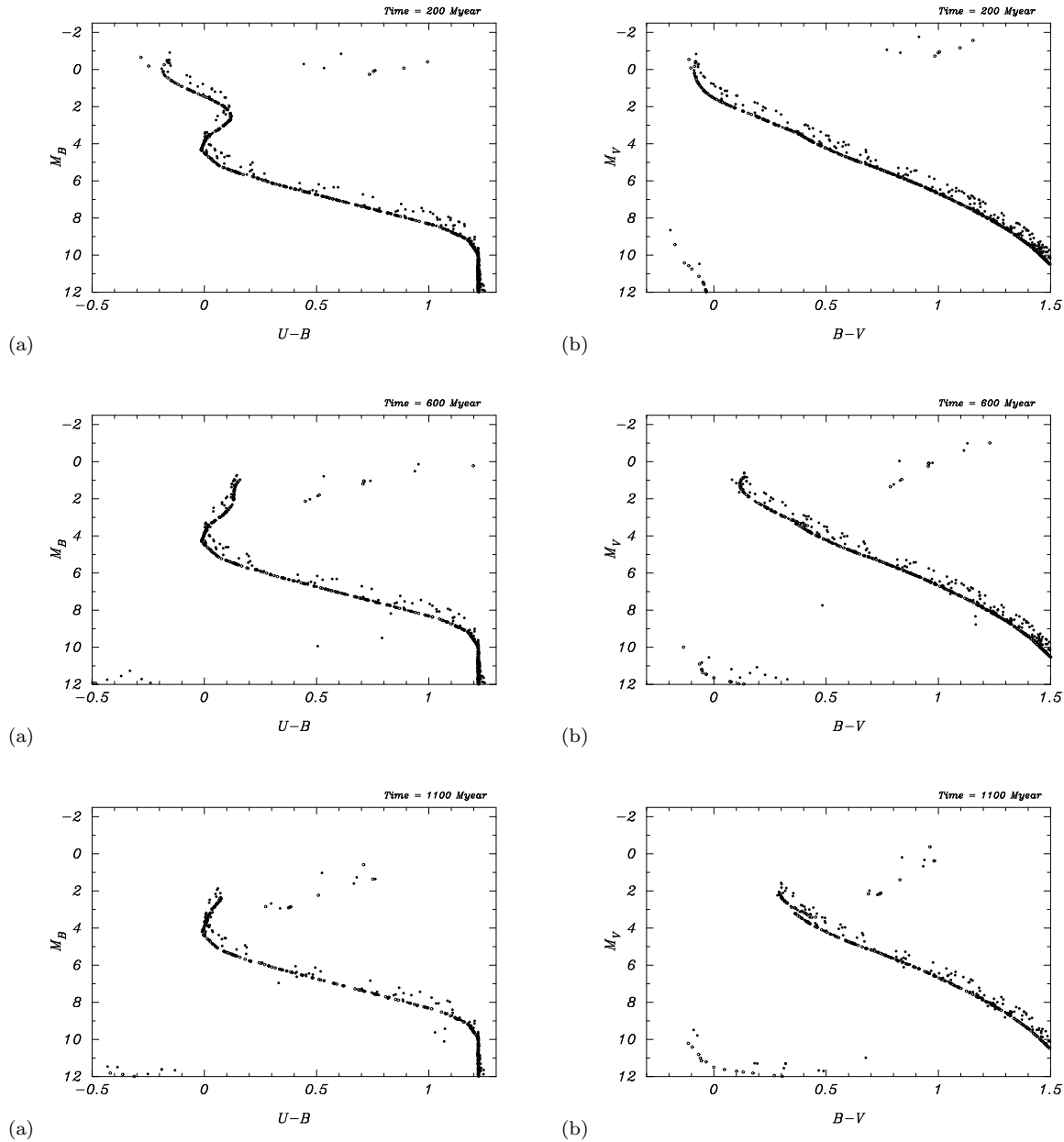


Figure 9. Hertzsprung–Russell diagram of all stars in model W6-III at ages of 200 Myr $U - B$ in the left panels and $B - V$ in the right panels (upper panels; 1983 objects), 600 Myr (middle; 1603 objects), and 1100 Myr (lower panels; 1009 objects).

to mass segregation. Most are a consequence of the evolving binary population, and will be discussed in more detail in Paper IVb. The inner HRD has a clear excess of (sub)giants and white dwarfs relative to the HRD at the half mass radius or that in the halo. Also, the turnoff region is more heavily populated in the inner HRD than in the others. Striking also is the lack of a clear binary sequence in

the outer Hertzsprung–Russell diagram. The bottom of the main-sequence is less clearly affected by mass segregation.

3.4 Blue Stragglers

The (small) numbers of blue stragglers do not depend strongly on the particular region of the cluster under study. We count four blue stragglers in the inner Hertzsprung–

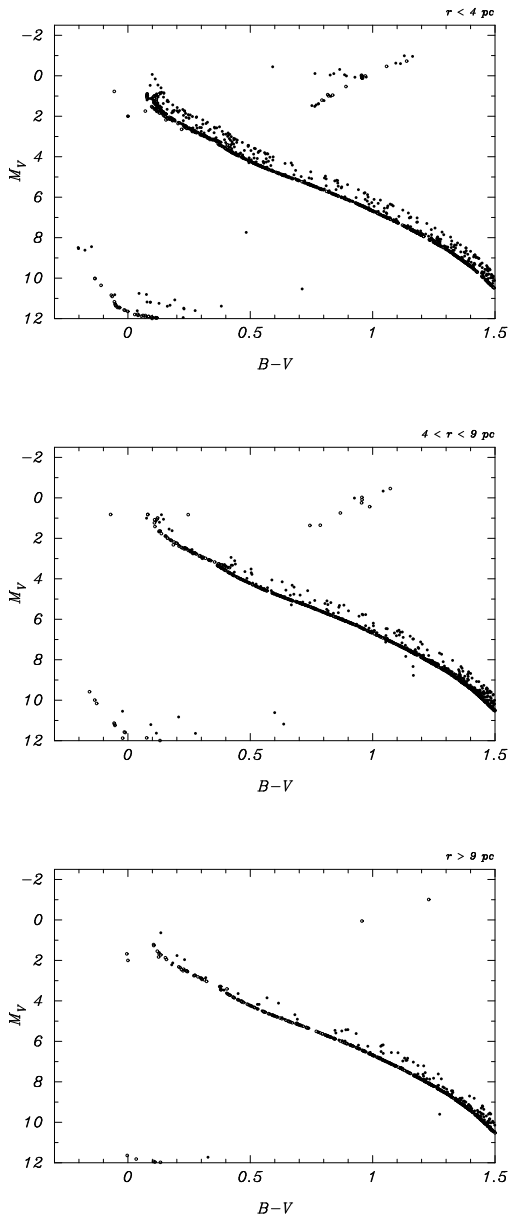


Figure 10. Hertzsprung–Russel diagrams of the combined W6 models at an age of about 600 Myr. The upper panel shows the innermost (non-projected) 4 pc (2004 objects), the middle panel stars between 4 and 9 pc from the cluster center (2658 objects), and the bottom panel stars more than 9 pc from the center (2039 objects).

Russel diagram, and one and two in the middle and outer frames of Figure 10, respectively. These numbers are fairly typical of our simulated clusters and also quite typical for the numbers observed (see Tab. 1). Fig 11 presents a graphical representation of the blue stragglers in model W6-III. (A

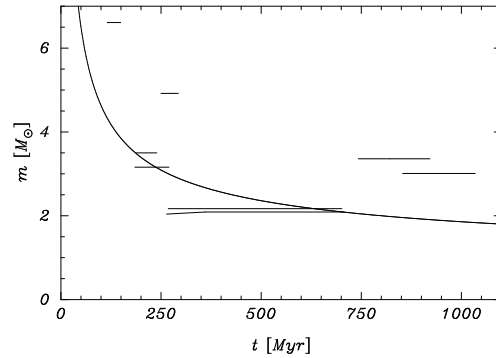


Figure 11. Blue stragglers in model W6-III. The solid curve gives the turnoff mass (in M_{\odot}) as a function of time (in Myr). The horizontal lines represent the tracks of the blue stragglers in model W6-III. The tracks start when the star is rejuvenated (see Appendix B), and stop when the blue straggler leaves the main sequence.

main-sequence star is identified as a blue straggler as soon as its mass exceeds the turnoff mass for that epoch.)

Most blue stragglers are the result of mass transfer in a close binary. In about half of all cases (37 out of 76 blue stragglers formed in all calculations performed), the mass transfer is unstable, leading to a merger. Blue stragglers formed from a stable phase of mass transfer are generally accompanied by a white dwarf or helium star (the young remnant of mass transfer, see Figure 11), causing the blue stragglers to lie slightly blueward of the turnoff in the Hertzsprung–Russel diagram (see §3.3).

Three blue stragglers formed via collisions in which a third star interacted with and became bound to binary, leading to a collision between the binary components. The orbit of such a blue-straggler binary is generally quite eccentric, and the companion to the blue straggler is most likely to be a main sequence star. Observing a blue straggler in an elliptical orbit around a stellar (main-sequence) companion would provide strong evidence for such dynamical interactions in star clusters (see Portegies Zwart 1996).

In none of our calculations a blue straggler with more than twice the turn off mass was formed i.e., there were no collisions between three or more stars. A discovery of a blue straggler with a mass more than twice the turn-off mass would provide strong evidence for effects of stellar dynamics, though one could imagine a primordial triple to get into a common-envelope situation in which all three stars spiral in to a triple merger. Portegies Zwart et al. (1999) find runaway collisions between more than two stars in their simulations of dense stars clusters without primordial binaries. Their results, however, are applicable for a different range of initial conditions, as they studied the dense and young central star clusters R 136 in the 30 Doradus region of the Large Magellanic Cloud.

Many blue stragglers experience mass transfer or a collision long before actually being classified as blue stragglers by our criterion (i.e. exceeding the turnoff mass). In most of these cases, one or more phases of mass transfer (stable or unstable, or even accretion from the stellar wind of a companion) has rejuvenated one of the stars in a close binary system (see Appendix B). As the cluster ages, the star remains behind on the main sequence, and eventually becomes identifiable as a blue straggler (see also paper II). This is illustrated in Figure 11 (the two long tracks with $m \sim 2$ and the track near $m \sim 3$).

A blue straggler which was rejuvenated long ago may show no trace of the event that caused its rejuvenation. Apart from residing above the turnoff, the star may appear completely normal; anomalous atmospheric abundances will have had sufficient time to mix with the stellar interior. In addition, if the blue straggler is rejuvenated only a little, the maximum distance on the Hertzsprung–Russel diagram between the cluster turnoff and the blue straggler will be very small; such a star may remain unidentified as a blue straggler. This may happen if mass transfer is unstable but does not lead to a merger, or if a binary is too wide for Roche-lobe overflow, and the blue straggler is rejuvenated by accreting a small portion of its companion’s stellar wind.

The lifetime of a blue straggler depends on the epoch at which it formed. Blue stragglers that form later are generally products of lower-mass stars, and tend to live longer than blue stragglers that formed early in the evolution of the stellar system.

3.5 Isophotes

Figure 12 shows a series of isophotes, as seen from various directions, for model W6-III at an age of 600 Myr. The Galactic center is located to the $-x$ direction (at a distance of about 12.1 kpc—see Table 4), and z points toward the Galactic north pole. While the cluster is barely flattened at birth,[§] by 600 Myr the cluster is significantly flattened by the Galactic tidal field. As expected, the flattening is greatest along the z axis, and also noticeable in the y direction.

Figure 13 shows images of model W6-III at three different moments in time. The images are created using a ray-tracing technique.

3.6 Escaping stars

Stars escaping from the cluster are lost primarily near the first and second Lagrange points. Figures 14 and 15 show the positions and projected velocities of the first 100 escapers from the system, and the 100 stars which escaped between

[§] This is simply a consequence of the fact that only the outermost parts of the cluster, near the Jacobi surface, show significant flattening, and these are initially very sparsely populated. Only when cluster evolution drives many stars out to the Jacobi radius does the flattening become readily apparent.

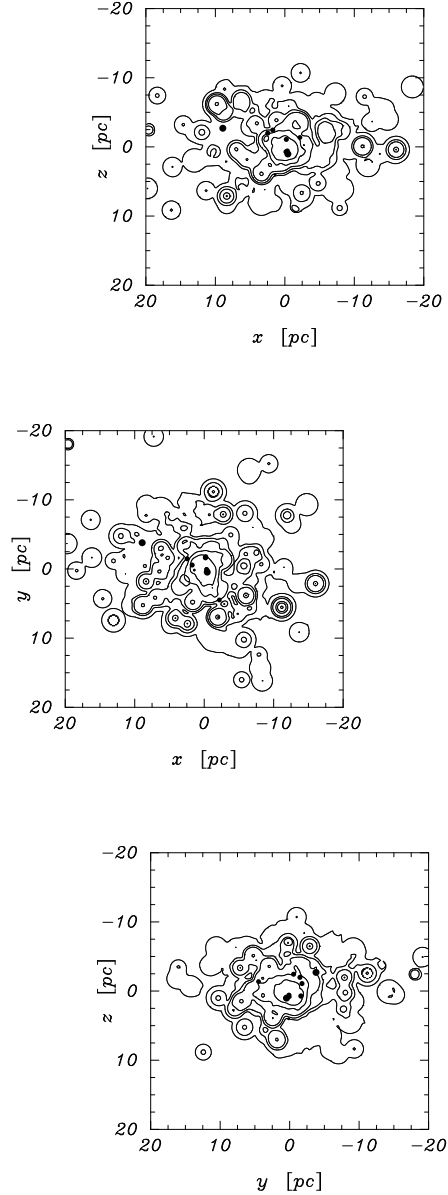


Figure 12. Isophotes in M_V for model W6-III at a cluster age of 600 Myr. The three panels present views along the three coordinate axes. The 10 (sub)giants are plotted as dots with size proportional to magnitude (and are excluded from the isophotes). The brightest region in the continuum plot has a surface brightness of -2.2 mag/pc^{-2} . Contours are plotted at $-0.86 \text{ mag pc}^{-2}$, 0.34 mag pc^{-2} , 1.6 mag pc^{-2} , 2.8 mag pc^{-2} , 4.1 mag pc^{-2} , and 7.8 mag pc^{-2} . Stars are assigned a Gaussian point spread function with a dispersion of 0.35 pc.

figure W6III0Myr.jpg
figure W6III622Myr.jpg
figure W6VT1512Myr.jpg

Figure 13. Visualization of model W6-III at zero age (top image), at an age of 622 Myr and at an age of 1512 Myr. Images were created using a ray-tracing technique.

$t = 550$ and $t = 650$ Myr. The left and right panels show, respectively, projections onto the $x - z$ and $x - y$ planes. The first and second Lagrange points lie on the x -axis, at distances of ~ 20 ($t = 0$) and ~ 17 ($t \sim 600$) pc from the cluster center. The small overall rotations of escapers evident in the $x - y$ projections are consequences of the Coriolis force acting on stars in the rotating frame of reference in which we perform the simulations. The high-speed escapers with roughly isotropic velocities in Figure 14 are escaping neutron stars, which receive high kick velocities on their formation. They are absent in Figure 15, as the cluster is by that time too old for supernovae to occur (except for type Ia supernovae).

The main differences between Figs. 14 and 15 are (1) the considerably larger spread in velocities, (2) the larger extent in z of the region over which stars are lost, and (3) the higher speeds of escaping stars at the earlier epoch. These differences are readily explained by a combination of effects; the evolution of the cluster in the Galactic tidal field, the presence of primordial binaries and the formation of neutron stars. As the cluster ages it becomes less massive and the Galaxy’s gravitational pull becomes relatively stronger. The tidal radius shrinks and the cluster velocity dispersion decreases, so the speed of escaping stars and their distances above or below the Galactic plane also decrease. The older cluster also lacks massive stars and no stars are ejected via supernova explosions. The shallow core collapse during the first 100 Myr results in increased binary activity, which also contributes to the higher stellar ejection speeds at the earlier time.

3.7 Stellar populations

Tables 6 and 7 present, for several cluster ages, the numbers of single stars and binaries by generic stellar types. The numbers are averaged over the calculations performed for each set of initial conditions, chosen with a different random seed from the same probability distribution. Table 8 gives the same data for a population of evolving binaries without dynamics, calculated using SeBa (see Appendix B).

Overall, the evolutionary differences in the populations of single stars and binaries between models W6 and W4 are quite small. Clearly, as already noted, the W4 clusters evaporate more rapidly (Figure 1), resulting in a generally more rapid decrease in the numbers of both stars and binaries. A more significant difference between Tables 6 and 7 is the larger numbers of white-dwarf binaries in the W4 models compared to other stellar types. Table 8 presents the stellar

Table 6. Stellar and binary types in the W6 models at various times. Binaries which contain two main-sequence stars are identified as (ms, ms), (ms, gs) contain a main-sequence star and a giant, (gs, gs) contains two giants, (gs, wd) contains a giant and a white dwarfs and (wd, wd) contains two white dwarfs. A bracket indicates the binary component which fills its Roche-lobe and is in a state of mass transfer to its companion star. binaries with neutron stars or black holes are omitted. The bottom row gives the binary fraction.

# runs:	5	5	5	5	4	4
time [Myr]:	0	100	200	400	600	800
ms	1024	939	915	830.4	914.5	508.5
gs	0	3.2	3.8	5.0	6.0	4.5
wd	0	4.8	9.4	21.2	33.3	26.3
(ms, ms)	1024	688.6	644.2	603.0	520.5	438.0
[ms, ms]	0	4.2	3.4	3.2	3.3	2.5
(ms, wd)	0	1.0	2.4	5.4	8.8	9.5
(gs, ms)	0	0.4	2.4	1.6	4.3	2.8
(gs, gs)	0	0.0	0.4	0.2	0.3	0.3
(gs, wd)	0	0.4	0.4	0.6	1.5	2.0
(wd, wd)	0	0.0	1.2	3.6	6.0	7.5
f_{bin}	0.5	0.42	0.41	0.42	0.36	0.46

Table 7. Stellar and binary types in the W4 models.

# runs:	5	5	5	5	2	2
time [Myr]:	0	100	200	400	600	800
ms	1024	998.8	938.8	771.2	604.5	164.0
gs	0	2.8	4.2	7.4	9.8	7.5
wd	0	4.2	9.4	20.6	33.5	31.0
(ms, ms)	1024	502.8	600.6	453.0	333.0	187.5
[ms, ms]	0	4.8	4.1	2.8	2.3	1.1
(ms, wd)	0	1.8	2.2	2.4	5.5	6.0
(gs, ms)	0	0.6	2.4	1.2	2.5	3.0
(gs, gs)	0	0.0	0.0	0.2	0.0	1.0
(gs, wd)	0	0.4	0.6	0.4	1.0	0.0
(wd, wd)	0	0.2	1.6	3.0	4.0	5.0
f_{bin}	0.5	0.34	0.39	0.37	0.35	0.50

and binary properties of an evolving population of isolated binaries. The differences between these binaries and the dynamically evolving population is considerable. Comparing Table 8 with Tables 6 and 7 reveals that the dynamically evolving populations are enhanced in both giants and white dwarfs; the effect is stronger in the W4 models because of the enhanced escape of the lighter stars.

Table 9 gives the fractions of various types of stars and binaries in the dynamical calculations, relative to the corresponding numbers from the population synthesis studies. The latter are normalized to the same numbers of single main-sequence stars and main-sequence binaries as in the initial dynamical calculations. (This normalization is employed here to show trends which are hard to see in the

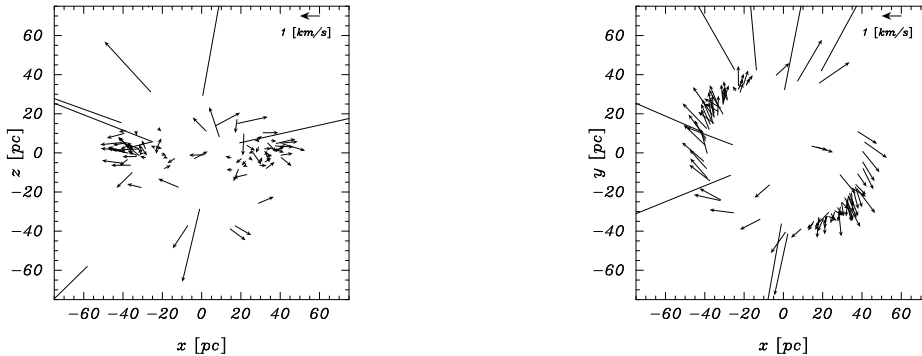


Figure 14. Vector diagram of the first 100 ($t < 218$ Myr) stars escaping from model W6-III. Projections onto the $x - z$ plane and the $x - y$ plane are shown. A velocity scale is shown in the upper right corner.

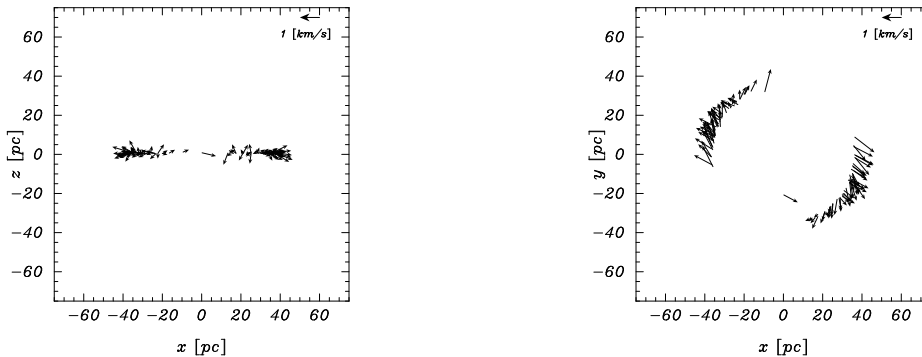


Figure 15. As for Figure 14, but for the 100 stars escaping from model W6-III between $t = 550$ Myr and $t = 650$ Myr.

Tables 6, 7 and 8.) Neutron stars and black holes are omitted from the comparison because the differences are directly obvious: Neutron stars escape from open star clusters, but they are retained in the non-dynamical models. Black holes are omitted because of their small numbers.

Although the numbers of giants and white dwarfs are also small, a trend is clearly visible: Single white dwarfs and dwarfs in binaries are overrepresented at later stages in the dynamical calculations, especially for the W4 models. The basic reason for this overabundance of white dwarfs and giants is their larger mass, which makes them more likely to be retained by the cluster. White dwarfs have a very complicated evolution within the stellar system, their progenitors being among the most massive objects while on the main sequence and the giant branch, but the white dwarfs having masses comparable to the mean once their envelopes are lost. White dwarfs are therefore preferentially formed in the cores of star clusters. Once the white dwarf is formed, it is hard to extract it from the core. These effects are more pronounced in smaller clusters ($t_{\text{rlx}} \lesssim 1$ Gyr). The W4 models

retain more white dwarfs than the W6 models because the latter relax on a longer time scale and evolve dynamically less rapidly than the former.

4 COMPARISON WITH OBSERVATIONS

4.1 The Pleiades

Figure 16 shows the M_I -magnitude luminosity function for the inner part of the Pleiades cluster (Hambly & Jameson 1991) and compares it with our model luminosity functions at 100 Myr.

The best fit between the observed and model luminosity functions is obtained for the stars within the half mass radius. This suggests that some mass segregation has already occurred in this clusters. Raboud & Mermilliod (1998) also find evidence for mass segregation in this cluster. Our luminosity function has too many bright stars and to make a reasonable fit we have to exclude stars with $M_I < 4.5$ from the sample. We are not sure why this is the case, but argue

Table 8. Stellar types from population synthesis studies of 1.5×10^5 binaries. The numbers of binaries is renormalized to 1024 because this is the number of primordial binaries in each of our dynamical calculations. The evolution of population of 1024 single stars was presented in Tab.2. Note that the dynamical models were performed with 1024 primordial binaries and 1024 single stars. We added the extra class of binaries which includes a neutron star or a black hole, such binaries are omitted in the dynamical models due their small number.

time [Myr]:	0	100	200	400	600	800
ms	0	0.79	0.42	0.92	0.34	0.31
gs	0	0.44	0.51	0.73	1.10	1.11
wd	0	0.87	1.96	3.57	4.99	6.55
ns/bh	0	4.37	4.42	4.42	4.43	4.43
(ms, ms)	1024	985.14	976.72	965.18	956.62	949.82
(ms, gs)	0	1.81	3.01	4.45	4.82	4.44
(ms, wd)	0	1.89	4.35	8.48	12.25	15.67
(ms, ns/bh)	0	0.10	0.08	0.05	0.05	0.04
(gs, gs)	0	0.13	0.25	0.24	0.27	0.24
(gs, wd)	0	0.27	0.78	1.33	1.59	1.63
(gs, ns/bh)	0	0.01	0.01	0.01	0.00	0.00
(wd, wd)	0	0.52	1.98	4.55	6.78	8.81
(wd, ns/bh)	0	0.27	0.25	0.23	0.22	0.20
(ns/bh, ns/bh)	0	0.11	0.10	0.10	0.09	0.09

Table 9. Relative numbers of stars and binaries in the dynamical models, as fractions of the numbers found in the non-dynamical population synthesis studies. The normalization is such that the dynamical and non-dynamical calculations contain equal numbers of single main-sequence stars and main-sequence binaries. Numbers greater than 1 indicate excesses of those stellar type in the dynamical calculation; numbers less than 1 represent depletion.

time [Myr]:	Normalized data for the W6 models					
	0	100	200	400	600	800
ms	1	1	1	1	1	1
(ms, ms)	1	1	1	1	1	1
gs	0	1.0	0.9	0.9	0.9	1.3
wd	0	1.4	1.0	1.3	1.2	1.3
(ms, gs)	0	0.3	1.1	0.6	1.2	1.3
(ms, wd)	0	0.8	0.8	1.0	1.0	1.3
(gs, gs)	0	0.0	2.3	1.3	1.3	2.4
(gs, wd)	0	2.1	0.7	0.7	1.3	2.6
(wd, wd)	0	0.0	0.9	1.2	1.2	1.8

time [Myr]:	Normalized data for the W4 models					
	0	100	200	400	600	800
ms	1	1	1	1	1	1
(ms, ms)	1	1	1	1	1	1
gs	0	1.0	1.0	1.5	2.3	6.3
wd	0	1.2	1.0	1.3	1.9	4.6
(ms, gs)	0	0.6	1.2	0.5	1.4	3.3
(ms, wd)	0	1.7	0.8	0.6	1.2	1.8
(gs, gs)	0	0.0	0.0	1.6	0.0	2.2
(gs, wd)	0	2.6	0.1	0.6	1.7	0.0
(wd, wd)	0	0.9	0.5	1.3	1.6	2.7

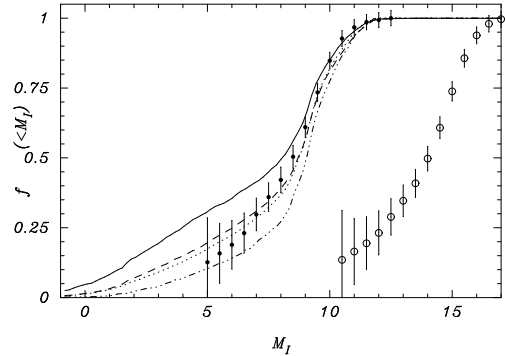


Figure 16. Cumulative luminosity function in M_I -magnitudes. The open circles (\circ) with (Poissonian) error bars show the apparent luminosity function for the Pleiades (Hambly & Jameson 1991). The corrected absolute luminosity function, assuming distance modulus $m-M = 5.5$ (Gatewood et al. 1990) is indicated by filled circles (\bullet). Both luminosity functions are corrected for the 50 stars brighter than $m_I = 10.5$ (Pinfield et al 1998). The dotted line is the initial luminosity function for all stars in the models (assuming that binaries are unresolved). The solid and dashed lines show the luminosity function for all models at $t = 100$ Myr within a projected (onto the $y-z$ plane) 25% Lagrangian and the half mass radius of the cluster. The dash-3dotted line give the luminosity function for the cluster stars in the outer 90% Lagrangian radius.

that the brightest stars were possibly overexposed in the observations, and may therefore have been omitted from the observed luminosity function.

The Pleiades is flattened, with an observed ellipticity $\epsilon \equiv (1 - b/a)$ of 0.17. Taking into account the orientation of the cluster in the tidal field of the Galaxy, Raboud & Mermilliod (1998) derive an intrinsic ellipticity of almost 0.3 (see also van Leeuwen et al. 1986), comparable to what we find in our models (see Figure 12) by comparing the distance to the Jacobi surface along the z axis with the distance to L_1 : $\epsilon \simeq 1 - r_z/r_J$.

4.2 Praesepe

Figure 17 shows the M_R -magnitude global luminosity function for the W6 clusters at birth and at 800 Myr and compares that with the observed luminosity function for Praesepe reported by Hambly et al. (1995a, 1995b), which is shown as filled circles with error bars.

The two 800 Myr old luminosity functions are taken from the stars within the projected half mass radius and stars farther away. The outer luminosity function (dashes) fits better to the bright stars where the inner luminosity function fits better to the dimmer stars. Again we can argue that omitting the brightest stars from the sample provides a better fit to the observations, in which case the luminosity

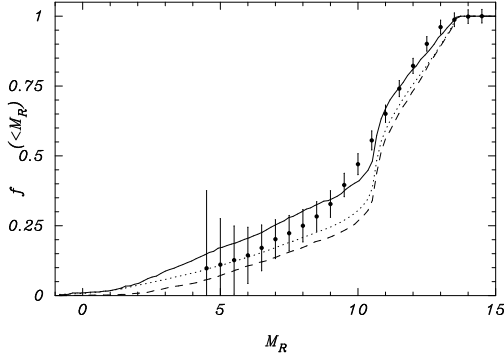


Figure 17. Cumulative luminosity function (M_R -magnitude) of the Praesepe cluster. The filled circles with error bars give the observed luminosity function within the half-mass radius (Hambly et al. 1995a, 1995b), to which 170 stars with $M_R < 4.5$ were added. The model W6 luminosity function for all stars at zero age is shown as a dotted line. The solid and dashed lines give the luminosity functions for models W6 at 800 Myr within and outside the projected (on the y - z plane) half mass radii.

function of the inner half of the cluster provides a better comparison.

4.3 The Hyades

Figure 18 compares the M_I -band luminosity functions for the stars and binaries of several models, at birth (dotted line) and at 600 Myr (other lines), with the observed luminosity function of the Hyades (Reid & Hawley 1999). Reid & Hawley observed the entire cluster and their luminosity function reportedly extends down to the hydrogen-burning limit. The $W_0=4$ data for the entire cluster (solid) and the $W_0=6$ model for the stars within the half mass radius (dash-3dot) does not fit as well as the data for model $W_0=4$ for stars within the inner half mass radius (dashes). Our models W6 are somewhat farther from the Galactic center than is the Hyades, which would tend to suppress mass segregation somewhat by increasing the cluster tidal radius. The $W_0=4$ models do exactly the opposite. Based on these arguments we conclude that Hyades is somewhat more mass segregated than our models predict and some degree of primordial mass segregation seems to be required.

Oort (1979) compared observations of Hyades with Aarseth's (1973, 1975) N -body calculations and concluded that the outer 4 pc of the Hyades cluster are more strongly flattened, with $\epsilon \simeq 0.5$, than the N -body models implied. The orientation of the Hyades in the Galaxy relative to the position of the sun then implies that the intrinsic flattening is even greater. Our calculations do not support Oort's conclusion, and a flattening of $\epsilon = 0.5$ is quite consistent with our N -body models. The reason for the discrepancy between our results and the conclusion of Oort is based on Aarseth's

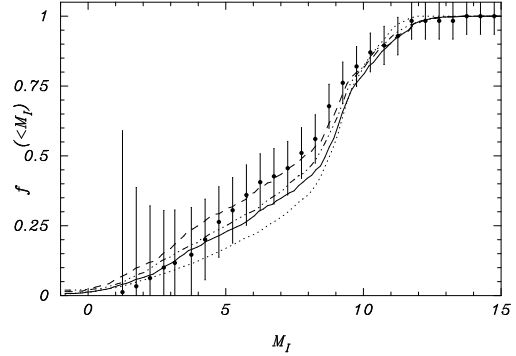


Figure 18. Cumulative M_I -magnitude luminosity function (filled circles with error bars) of the Hyades star cluster (Reid & Hawley 1999). The dotted line is the initial luminosity function for all stars in the model calculations. The solid line and dashed lines give the luminosity function for model W4 at an age of 600 Myr for stars within the projected (on the y - z plane) tidal radius (solid) and within the half-mass radius (dashed). The dash-3dotted line gives the same data as the dashed line but then for model W6.

models which were computed with a very small number of stars. The flattening of the cluster in the tidal field of the Galaxy, however, becomes more apparent towards the clusters' tidal radius which has smallest stellar density. Calculations which are performed with a limited number of stars $\lesssim 500$ will hardly show the flattening in the tidal field.

4.4 NGC 3680

Figure 19 compares the observed M_V -band luminosity function of the old open cluster NGC 3680 with our model luminosity functions. The observed luminosity function is poorly reproduced by our cluster models. However, if we remove the least luminous stars (those with $V > 11.5$), the 1.4 Gyr model fits the observed luminosity function fairly well. The imposed lower limit is rather arbitrary, it suggests that the observations may not properly correct for the faintest stars, or they may simply be absent from the data. Mass segregation generally causes the lightest stars to escape from the cluster which, in time, leads to an overabundance of massive stars. The observed clusters, however, seem to have too few high mass stars and also too few low mass stars, which is hard to understand from a dynamical point of view. We therefore argue that in this case the lack of low mass stars is an observational selection effect.

4.5 Isophototes

Figure 20 shows isophotes of the clusters NGC 2287, NGC 2516 and NGC 3680. NGC 3680 is most strongly flattened ($\epsilon \sim 0.23$), the other two are more circular in appearance; NGC 2287 has $\epsilon \sim 0.05$ and NGC 2516 has $\epsilon \sim 0.14$.

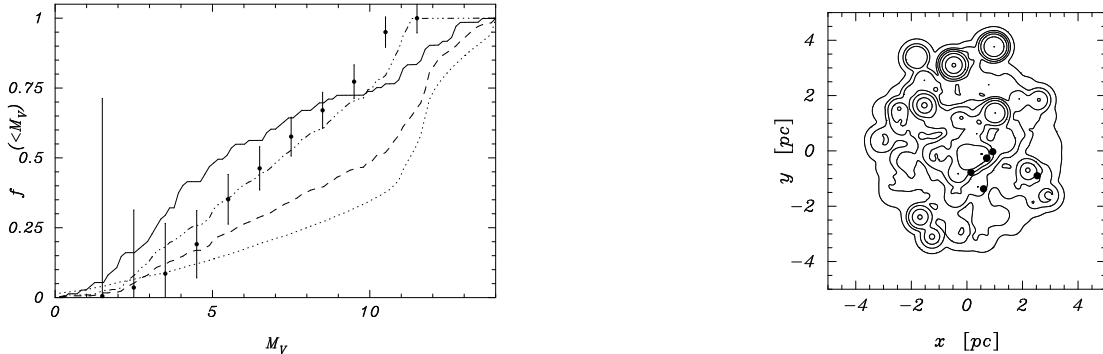


Figure 19. The filled circles with error bars show the observed cumulative luminosity function, corrected for field stars, of the star cluster NGC 3680 (Hawley et al. 1999). The dotted line gives the initial luminosity function for all models, all other lines show luminosity functions at 1400 Myr. The solid and dashed lines give the luminosity function for all stars within the half mass radius of model W4 and W6, respectively. The dash-3dotted line shows only the stars with $M_V < 11.5$ from the dashed line (within the half-mass radius of model W6 at 1400 Myr).

We measured these ellipticities for the inner 4 pc for each cluster.

The faintest stars in Figure 20 are 13th magnitude for NGC 2287 and 15th magnitude for NGC 2516 and NGC 3680. Taking the distances to these clusters into account, it is clear that only the top end of the main sequences are included in the isophotes. Since mass segregation causes these high-mass stars to be more centrally concentrated than lower-mass stars, it is likely that we see only the inner, roughly spherical, regions of NGC 2287 and NGC 2516 (see Figure 12). NGC 3680 appears much somewhat rectabgular on the image and we are tempted to explain this shape as a result of the limited imaging; is the cluster is truncated by the edge of the field of view?. In this case it is not surprising that this cluster appears somewhat flattened. If one looks at the inner density contours the cluster looks much more circular. Note also that the tidal radii for these clusters listed in Tab. 1, 13, 6.3 and 4.3 pc for NGC 2516, NGC 2287 and NGC 3680 respectively, seem inconsistent with the above pictures. The isophotes of NGC 2516 and NGC 2287 represent only the central portion, where for NGC 3680 appears much bigger than the tidal radius we derived in Tab. 1. The table possibly underestimates the tidal radius of NGC 3680.

5 COMPARISON WITH OTHER WORK

Table 10 compares the evaporation times of our model calculations with previously reported results. We discuss each in turn. Table 10 lists the initial conditions of the models with which we compare our own.

Terlevich (1987) performed direct N -body calculations

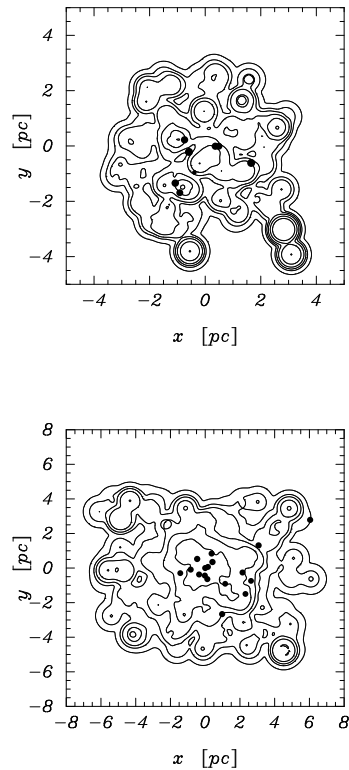


Figure 20. Isophotes in M_V of the cluster NGC 2516 (top panel) NGC 2287 (bottom left), and NGC 3680 (bottom right). The adopted distance moduli are 9.1, 8.2, and 9.95, corresponding to distances of 655 pc, 373 pc and 735 pc for the top and bottom left and right panels, respectively. The (sub)giants are plotted as filled circles; the remaining stars are plotted as isophotes. The central luminosity densities are -2.0 mag pc^{-2} , -2.2 mag pc^{-2} and $-0.54 \text{ mag pc}^{-2}$ for the top, bottom left and right panels, respectively. Contours are plotted at constant intervals of 1.25 mag. Stars are assigned a Gaussian point spread function with a dispersion of 0.06 pc (0.1 pc for the bottom figure), the figures contain 594, 178 and 738 stars for the top and bottom left and right panels, respectively.

Table 10. Overview of the model features, initial conditions and lifetimes of our model calculations and those reported by other workers. The Galactic tidal field may be modeled as that of a self-consistent disc (Disc) or a point mass (PM); initial density profiles are an anisotropic King model (AKing), an Isothermal sphere (Iso), or a Plummer sphere (Plummer) the latter two with a cut off. Stellar and binary evolution are indicated by + (included) or - (for neglected). Note: Terlevich and de la Fuente Marcos work in terms of the initial virial radius, which is typically about 20% bigger than the half-mass radius.

	Galaxy model	Density profile	Stellar evolution	Binary	N	$\langle m \rangle$ [M_{\odot}]	f_{bin}	r_{tide}	r_{hm}	t_{rlx}	t_{end}	$t_{\text{end}}/t_{\text{rlx}}$
								[pc]		[Myr]		
W4	Disc	AKing	+	+	3072	0.56	50	6.3	2.14	109	1200	11.0
W6	Disc	AKing	+	+	3072	0.54	50	12.1	2.00	102	~ 1600	15.7
Terlevich	Disc	Iso	+	-	1000	0.50	0	12.1	2.00	71	~ 1400	19.7
McMillan & Hut	PM	Plummer	-	-	2048	1	10	16.5	2.06	86	2500	29.0
Kroupa	PM	Plummer	+	-	400	0.32	100	6.5	2.53	77	693	9.0
de la Fuente Marcos	Disc	Iso	+	-	750	0.60	33	9.9	2.47	67	1061	15.8

with up to 1000 stars, including a power-law stellar mass function, mass loss from single-star evolution, and the tidal field of the Galaxy. The implementation of the Galactic tidal field and the evolution of single stars were somewhat similar to those presented in this paper. Her model XII had initial conditions most similar to our own, although some significant differences exist. Terlevich’s models started with spherical distribution of stars with density proportional to $1/r^2$, virial radius 2 pc (half-mass radius of about 1.6 pc), and located at a distance of 10 kpc from the Galactic center. The resulting half-mass crossing time was 5.2 Myr, comparable to the ~ 4.1 Myr in our models. Terlevich’s model XII initially consisted of 1000 stars drawn from a Salpeter mass function, with a mean mass of $0.5 M_{\odot}$. The initial virial radius was $Q \equiv E_{\text{kin}}/|E_{\text{pot}}| = 0.25$, less than equilibrium value of 0.5. Even though the model started with fewer stars, the cool initial conditions mean that the initial relaxation time was comparable to that in our own models. The half-life of model XII was 770 Myr. The run was terminated at 1 Gyr, by which time about 70% of the mass had been lost. We estimate that the cluster would have dissolved in about 1.4 Gyr.

The half-mass lifetimes of our W6 models are all around 800 Myr, similar to that of Terlevich’s model XII. This is somewhat surprising, as we might have expected that our W6 models, with more stars, would live longer than the comparable models of Terlevich. The reason for this discrepancy cannot be attributed to the large fraction of primordial binaries in our calculations, as binaries do not dramatically affect the evaporation rate of the cluster (Figure 1). The difference may possibly be due to the lower high-mass cutoff in Terlevich’s initial models. Although her model XII was initially less concentrated than our W6 models, it did reach core collapse. In general, more concentrated models tend to live considerably longer than shallower models (Takahashi & Portegies Zwart 2000).

The evolution to core collapse in Terlevich’s model XII was aided by the absence of stars with masses greater than $10 M_{\odot}$. By the time the turnoff mass has dropped below $10 M_{\odot}$ (after about 22 Myr) our W6 models have lost be-

tween 4% and 9% of their mass due to stellar evolution alone. The loss of even such a small mass fraction may have dramatic consequences for the further evolution of the stellar system, as this mass is lost from the most massive stars, which reside deep inside the cluster potential well. The shorter lifetime of clusters with large populations of massive stars is demonstrated by Terlevich’s model XV, where the initial mean mass was $7.4 M_{\odot}$ and the cluster did indeed dissolve much more rapidly.

The Galactic tidal field produced a similar flattening effect in Terlevich’s clusters as in our own (compare her Figure 7 with our Figure 12).

The simulations reported by McMillan and Hut (1994) included up to 2048 equal mass stars, including up to 20% rather soft primordial binaries, and incorporated the Galactic tidal field, modeled as the field of a distant point mass. However, they excluded stellar evolution and hence any possibility of stellar mass loss. In the absence of a physical time scale associated with stellar evolution, they presented their results in units of the initial half-mass relaxation time. Our W6 models have half-lives of about 6 initial relaxation times, much shorter than the ~ 29 initial relaxation times for the most comparable McMillan & Hut models. Also, as discussed previously, all the McMillan & Hut models experienced core collapse, which is absent in our simulations.

The main reasons for these differences are the effects of stellar mass loss and the presence of a stellar mass function in the present studies. In our models, core collapse is arrested by mass loss. In addition, the McMillan & Hut models all started off well inside their tidal radii, significantly increasing their lifetimes.

In a continuing effort to understand the evolution of young open star clusters, Kroupa (1995a; 1995b; 1995c) performed N -body calculations with up to 400 stars, all of them members of primordial binaries. He adopted a distribution in orbital separation flat in $\log a$, but selected a between ~ 360 and $\sim 3.6 \cdot 10^5 R_{\odot}$; the binaries in his calculations were thus on average much wider than in our calculations. His models included the Galactic tidal field and stellar mass loss, but neglected binary evolution.

Kroupa’s model with the highest initial relaxation time started from a Plummer sphere with a half-mass radius of 2.5 pc and a crossing time of ~ 20 Myr. It dissolved in about 700 Myr. Scaled to the initial relaxation time, this is somewhat faster than our W4 models. The main reasons for this more rapid evaporation are most probably the shallower initial density profile in his models and the cluster’s smaller distance from the Galactic center.

We compare the binary and triple properties of our models with those of McMillan & Hut and Kroupa in more detail in Paper IVb.

De la Fuente Marcos (1997) studied the effect of the initial mass function on the dynamical evolution of open star clusters, including both stellar mass loss and the tidal field of the Galaxy. His calculations were limited to 750 stars and included 33% rather wide primordial binaries, all with a mass ratio of 0.5, in which (binary) evolutionary effects were neglected. His model XX used Scalo’s (1986) mass function and had an initial virial radius of 2.47 pc. The initial relaxation time for this model was about 67 Myr; the crossing time was 7.5 Myr. This model dissolved in about 1 Gyr, slightly faster than our models. However, scaled to the initial relaxation time, this result is consistent with the dissolution time of our W6 models (see Table 10).

6 SUMMARY AND DISCUSSION

The aim of our simulations is to study the evolution of open star clusters such as the Pleiades, Praesepe and the Hyades. These clusters differ significantly in age, but have comparable physical characteristics, stellar membership, total magnitude and internal velocity dispersions. Our N -body calculations incorporate, in a fully self-consistent fashion, mass loss from single stars, binary evolution, dynamical encounters among single stars and binaries and the effect of the Galactic tidal field.

We have compared the luminosity functions, isochrones and projected luminosity profiles of our models with observations. For some clusters, it is hard to find a good match between model and observed luminosity functions. Mass segregation and observational limitations significantly reduce our ability to find a match, and restrict our understanding of the differences we see. However, we find that for models for which we compared the luminosity functions with Praesepe and the Hyades, the observations show evidence for significantly more mass segregation than is seen in the models. We conclude that these clusters may have been born somewhat mass segregated. Alternatively these clusters may have started out somewhat more massive than assumed here, but with a shallower density profile. The selective evaporation of lower mass stars then results in a “dynamically old” appearance (see also Takahashi & Portegies Zwart 2000).

The global luminosity function of Praesepe and its degree of mass segregation suggest an age greater than 800 Myr, which is at the high end of the observed range. The luminosity function of NGC 2287 is consistent with the

observed age of 150–200 Myr. Our age estimates for the Pleiades and Hyades, based on the structure and dynamical state of these clusters, are consistent with ages derived from isochrone fitting.

6.1 Mass segregation

The first effects of mass segregation in our models are discernible in the cluster core after only a few million years, a small fraction of an initial half-mass relaxation time. After about a relaxation time, mass segregation becomes measurable in the cluster outskirts. The luminosity function of the inner parts of the cluster provides a useful tool for studying mass segregation, although one has to select regions which are well separated in radius in order to make the effect visible. As expected, giants and binary stars are most strongly affected by mass segregation and it is easiest to identify the effect by comparing the radial distribution of giants with that of the lower mass main-sequence stars.

One important effect of mass segregation is that older clusters become rich in white dwarfs and giants relative to the Galactic field. These stars may be single or members of binary systems. The main reason for the overabundance of giants and white dwarfs in clusters is the depletion of low mass main-sequence stars by evaporation. This flattening of the mass function due to mass segregation has also been studied by Takahashi & Portegies Zwart (2000) for more massive clusters. They also find that clusters which are close to disruption are rich in compact objects and giant stars.

The W4 models have shallower initial potentials, lie closer to the Galactic center, and are more strongly affected by mass segregation because of their more rapid evaporation. We suggest that the best place to look for evidence of mass segregation is in star clusters with larger half-light radii, which have shallower potentials. Since mass segregation manifests itself more clearly in dynamically evolved systems, it is also better to look at older clusters. A relatively old cluster (age $\gtrsim 500$ Myr) with a relatively small mass ($M_{\text{tot}} \lesssim 500 M_{\odot}$) would be ideal.

6.2 Age estimates

The “dynamical ages”[¶] of our model clusters are often inconsistent with ages determined by isochrone fitting. The instantaneous relaxation time is a poor estimator of a cluster’s dynamical age. The cores of star clusters lose their memory of the initial relaxation time within a few million years, well within an initial half mass relaxation time, but the time scale for global cluster amnesia to set in is far larger than the initial relaxation time. The half-mass relaxation time tends to increase by a factor of two or three, reaching a maximum

[¶] We define the dynamical age of a cluster as its lifetime expressed in units of the initial relaxation time.

near the cluster's half-life and decreasing thereafter. The increase is caused by the internal heating of the cluster; the decrease mainly by loss of stars.

6.3 Escaping stars

Stars tend to escape in the direction of the L_1 and L_2 Lagrange points of the Galaxy–cluster system. The velocities of the stars at these points are highly anisotropic and, as expected, pointing mostly radially away from the cluster center. The velocities of the escaping stars are comparable to the cluster velocity dispersion; very few stars are ejected with high velocities following a strong dynamical encounter.

Neutron stars are ejected isotropically and with much higher velocities, owing to the asymmetric kicks they receive during the supernovae that create them. Binaries containing the progenitors of neutron stars are generally disrupted by the first supernova explosion; in all the calculations presented in this paper, only one binary survived the first supernova. However, the existence of that single binary does suggest that it may be possible to form X-ray binaries in open clusters. Such binaries are only expected to exist in star clusters which are younger than ~ 45 Myr (the turnoff age of a $7 M_\odot$ star), because mass loss and the velocity kick imparted to the binary causes it to escape (see paper IVb).

Black holes are more easily retained by the cluster, but are very rare due to their high progenitor mass and the steepness of the Scalo initial mass function.

6.4 Tidal flattening

The tidal field of the Galaxy flattens the cluster significantly in the z direction, and to a lesser extent along the y axis. A cluster which is spherical at birth develops this flattening in its outer regions within a few crossing times; the inner parts remain fairly spherical. All our models show this flattening, but its observability from Earth depends on the orientation of the cluster in the Galactic plane.

Ellipticities reported for the Pleiades ($\epsilon \sim 0.3$; van Leeuwen et al. 1986) and Hyades ($\epsilon \sim 0.5$ in the outer regions; Oort 1979) are consistent with our model calculations. The available data for NGC 2287 and NGC 2516 do not show significant flattening. However, these data contain only stars from the innermost 3 pc, which are affected least by the Galactic tidal field. NGC 3680 appears more square than elliptical. This may be caused by the small field of view of the telescope, which could cause a star cluster to take on the shape of the CCD frame (see Fig. 20).

The flattening persists during mass segregation, in the sense that the mass-segregated Lagrangian radii are ellipsoids. Projection of the cluster onto the background may therefore decrease the observed mass segregation.

6.5 Core collapse

Our models experience rather shallow core collapse during their early evolution. The clusters then expand more or less homologously, preserving their initial density profiles. The expansion is driven by stellar mass loss and, to a lesser extent, by binary heating; dynamical models without stellar mass loss but which include a tidal field and primordial binaries do show core collapse (McMillan & Hut 1994). Once the cluster has lost a considerable fraction of its stars the system shrinks again. The remnant with a few remaining stars may become quite compact before it dissolves, but we find no evidence for late core collapse before complete disruption.

6.6 Giants and white dwarfs in open clusters

A cluster's single-star population is not noticeably affected by cluster dynamics until the age of the system exceeds ~ 2 initial half-mass relaxation times. However, the binary populations are measurably influenced by dynamics even at early times (see Paper IVb). At later times ($t \geq 400$ Myr), our model clusters tend to become rich in giants and white dwarfs. Small-number statistics on the giants limit the degree to which we can quantify this statement, but the white-dwarf populations in our models increased by factors of 1.3 to 4.6 (for model W6 and W4, respectively) relative to what one would expect for a non-dynamically evolving population of single stars and binaries. Most of the excess white dwarfs are members of binary systems.

Table 1 presents an overview of the numbers of white dwarfs observed in the clusters studied in this paper. Explaining the number of white dwarfs in the Hyades is a long-standing problem, starting with discussions in the mid-1970s by Tinsley (1974) and van den Heuvel (1975), and continuing into the 1990s (Eggen 1993; Weidemann 1993). All these papers conclude that the observed number of white dwarfs is too small, by about a factor of three, for the inferred cluster mass and age. The three leading explanations were: (1) the upper mass limit for the production of white dwarfs may be as low as $\sim 4 M_\odot$ (Tinsley 1974), white dwarfs are born with a velocity kick as neutron stars do (Weidemann et al. 1992) and (3) mass segregation selectively ejects white dwarfs (van den Heuvel 1975). By studying the white dwarfs in NGC 2516, Koester & Reimers (1996) firmly conclude stars up to $8 M_\odot$ can form white dwarfs, removing the first solution to this conundrum. However, our calculations are inconsistent with the idea that white dwarfs are preferentially ejected from star clusters. On the contrary, the white dwarfs in our simulations are more easily retained than main-sequence stars of the same mass, causing the older clusters to become relatively white-dwarf *rich* for their mass.

We can study this problem further by comparing the ratio of the number of white dwarfs to the number of giants: $f_{\frac{\text{wd}}{\text{gs}}} \equiv N_{\text{wd}}/N_{\text{gs}}$. For the first five open clusters in Tab. 1 this fraction ranges from $f_{\frac{\text{wd}}{\text{gs}}} = 1$ for NGC 2516 and the Pleiades

to $f_{\text{gs}}^{\text{wd}} = 2.5$ for the Hyades. For an evolving population of single stars without dynamics (see Tab. 2), we find that the ratio ranges from 1.1 at 100 Myr (the age of NGC 2516) to 4.2 at 600 Myr (comparable to the age of Hyades).

Binary evolution complicates the comparison due to an obvious selection effect—the giants can probably all be seen, but white dwarfs are easily hidden near a main-sequence or giant companion. We obtain estimates for $f_{\text{gs}}^{\text{wd}}$ in a field population with 50% primordial binaries by combining the single stars from Tab. 2 with the binaries from Tab. 8. We calculate an upper limit to $f_{\text{gs}}^{\text{wd}}$ by accounting for all white dwarfs [counting (wd, wd) binaries as two objects and including (ms, wd) and (gs, wd) binaries]. A lower limit is obtained by counting (wd, wd) binaries as one object and excluding white-dwarf binaries containing a main-sequence or giant companion. For the field (no dynamics) population, we find $f_{\text{gs}}^{\text{wd}} = 0.80\text{--}1.3$ at 100 Myr, and $f_{\text{gs}}^{\text{wd}} = 2.7\text{--}4.1$ at 600 Myr. Combining models W4 (Tab. 7) and W6 (Tab. 6) we obtain $f_{\text{gs}}^{\text{wd}} = 1.2\text{--}1.7$ at 100 Myr and $f_{\text{gs}}^{\text{wd}} = 3.0\text{--}4.0$ at 600 Myr.

The observed value of $f_{\text{gs}}^{\text{wd}} \sim 1$ at around 100 Myr seems somewhat low, but probably not inconsistent with our models. However, the value of $f_{\text{gs}}^{\text{wd}} \sim 2.5$ of the Hyades cluster (at about 600 Myr) is smaller than our models predict, suggesting that a considerable fraction of the white dwarfs are hidden in binaries.

The value of the fraction $f_{\text{gs}}^{\text{wd}}$ does not seem to pose a serious problem to understand any of the clusters discussed here. But according to the evolution of the field stars and binaries (combining Tabs. 2 and 8), at an age of 600 Myr we expect a total of about 15 giants and 59 white dwarfs. The comparable models W4 and W6 contain, respectively, 13 and 12 giants, and 48 and 57 white dwarfs at that age. Model W6 has lost about 40% of its mass and model W4 has lost about 60%, yet the numbers of giants and white dwarfs have decreased by only 4% – 20%. Averaging over time, we find a decrease in the number of giants and white dwarfs of about 2% per 100 Myr. Apparently, the dynamical evolution of these clusters has little effect on the number of giants and white dwarfs. (In fact, this was assumed by von Hippel [1998] in estimating the mass fractions of white dwarfs in open clusters.) Number counts of giants and/or white dwarfs may therefore provide a reasonable estimate of a cluster’s initial mass.

For a fifty-fifty mixture of single stars and binaries, meaning that 2/3 of the stars are binary components, the mean mass of a star is $\langle m \rangle = 0.46$ at $t = 100$ Myr, 0.41 at 600 Myr and almost constant ($\langle m \rangle \sim 0.40$) thereafter. We use the numbers of giants to estimate the initial masses of the star clusters in Tab. 1, because the giants are least plagued by selection effects (although their small numbers significantly limit the accuracy of our estimates). The number of giants per 1k stars is 2.7 at 100 Myr (see Tabs. 2 and 8), and rises rapidly to about 6.5 at 400 Myr, after which

the specific number of giants remains roughly constant. For an open cluster older than ~ 400 Myr, we thus estimate its initial mass via

$$M_0 = 65M_{\odot}N_{\text{gs}} \left(1 + \frac{0.02t}{[100\text{Myr}]} \right). \quad (1)$$

For younger clusters, the factor 65 ($= 1024 \times 0.41/6.5$) is larger—170 at 100 Myr and ~ 100 at 200 Myr.

We apply this method to the clusters from Tab. 1 with more than 5 giants and obtain the following birth masses: 830 M_{\odot} for NGC 2287, 3100 M_{\odot} for NGC 2660, and 1400 M_{\odot} for NGC 3680. These mass estimates seem reasonable. For NGC 2534, Praesepe and the Hyades, the mass estimates are 690 M_{\odot} , 370 M_{\odot} and 290 M_{\odot} , respectively, considerably smaller than the observed masses of these clusters (see Tab. 1).

The initial mass estimate for these clusters increases proportional to the number of giants. The ratio $f_{\text{gs}}^{\text{wd}}$ does not pose a serious problem and therefore, instead of too few white dwarfs, Hyades may have too few giants. Where white dwarfs can be hidden easily in binaries, giants are not that easy to hide. One way to decrease the number of giants is by binary activity. The number of giants can be decreased when subgiants are stripped in a phase of mass transfer before they reach the horizontal branch, where they spend most of their time. In order to reduce the number of giants in the fashion we require most binaries to be born with short orbital periods ($\lesssim 100$ days). Alternatively the giant lifetimes adopted in our models may be too long.

6.7 Notes on individual clusters

NGC 2516 deserves much more study, as its dynamical parameters (total mass, half-mass and core radii) are poorly known.

The Pleiades cluster has been quite thoroughly studied in searches for brown dwarfs and planets. Its mass function fits nice with the luminosity function from our models, with the exception that our models contain too many bright stars.

NGC 2287 is quite poorly studied, and with the quoted values for the tidal radius it has an extremely low mass for its age (see Table 1). The presence of 8 giants suggests that its mass must have been comparable to that of NGC 2516.

Praesepe has been studied recently in great detail, and appears to fit well with our dynamical models. However, the cluster is rather shallow and may have been born somewhat more massive and less concentrated ($W_0 \lesssim 4$) than our models. This conclusion is based on the observed shallow density profile and the high degree of mass segregation. There is some excess of stars with $V \sim 9\text{--}11$ is unexplained by our models. The observed cluster seems to be very deficient in giants. Based on the number of white dwarfs and the dynamical state of the cluster we would expect at least 20 giants in this cluster, where only 5 are known.

The Hyades cluster fits well with our models, indicat-

ing that it is possible to estimate the initial conditions for an observed star cluster rather accurately. The cluster does not appear to be deficient in white dwarfs if we compare them to the number of giants. However, if the mass of Hyades quoted in Table 1 is correct, the observed number of white dwarfs and giants seems too small by a factor of about three.

NGC 3680 Fits well with our W6 models expect for the luminosity function, which is deficient of low mass stars. A possible solution may be that these stars were initially absent in the cluster or that the observations do not go faint enough to reveal the low mass stars.

6.8 Comparison with other work

Our models evaporate on time scales generally consistent with dissolution times reported in previous calculations. The models of Terlevich (1987) and de la Fuente Marcos (1997) compare well with the evaporation times of our W6 models. Terlevich’s models evolve somewhat more slowly due to the lack of massive stars and the rather cool initial conditions, which drive the cluster to core collapse and therefore extend its lifetime somewhat. The models of McMillan & Hut (1994) dissolve more slowly than ours. This discrepancy can be completely explained by the absence of stellar evolution mass loss and binary evolution in their models, along with the small size of those models relative to the clusters’ tidal radii in the Galactic potential.

The only real discrepancy is in the work of Kroupa (1995a), whose models dissolve somewhat more rapidly than ours. Possibly the small numbers of stars and the large binary fractions drive a more rapid evaporation than one might naively expect. The evaporation rate of star clusters is known to depend on total the number of stars (Heggie et al. 1997; Portegies Zwart et al. 1998). In Section 1 we argue that the presence of primordial binaries has little effect on the cluster lifetime. It is, however, not clear how this trend propagates in the scaling of cluster lifetimes with respect to the number of stars.

APPENDICES

APPENDIX A: TERMINOLOGY

Throughout the paper (and in future papers in this series) we will use consistent nomenclature. Some of these terms are rather confusing and have been used by different authors in the past with slightly different meanings. For clarity we present here a short glossary of terms.

Binary fraction: throughout this paper we define the binary fraction as:

$$f_{\text{bin}} = \frac{N_{\text{bin}}}{N_{\text{sing}} + N_{\text{bin}}}. \quad (\text{A1})$$

Here N_{sing} and N_{bin} are the number of single stars and binaries.

Cluster center: The density center of the cluster, as defined below. Alternative definitions may use the number density or the luminosity density, or the point where the density is greatest, and may include projection effects.

Collision: A collision occurs when the distance between two stars i and j becomes smaller than the sum of their effective radii: $d < d_{\text{coll}}(r_i + r_j)$, with $d_{\text{coll}} = 1$. The effective radii are determined from detailed fluid-dynamical calculations.

Core radius: The weighted average distance of all stars from the density center. Casertano & Hut (1985): originally used a weighting proportional to the local density. However, in practice this definition is unsuitable for clusters with near-isothermal density profiles ($\rho \sim r^{-2}$). Following Aarseth (1986), we adopt the modified definition

$$r_{\text{core}} \equiv \frac{\sum_i |r_i - r_j| \rho_j^{(i)2}}{\sum_i \rho_j^{(i)2}}, \quad (\text{A2})$$

where ρ_j is given by Eq. A6. Note that this definition of the core does not *necessarily* have any simple relation to the “core radius” normally quoted by observers, nor to the “dynamical” core radius $r_c = \sqrt{\frac{3\langle v^2 \rangle_c}{4\pi G \rho_c}}$, where ρ_c and $\langle v^2 \rangle_c$ are, respectively, the cluster’s central density and velocity dispersion (Binney & Tremaine 1987).

Crossing time: The time taken by a star with velocity equal to the velocity dispersion v to cross the virial radius r of the stellar system $t_c = r/v$ which for practical reasons is written as

$$t_c \equiv \left(\frac{r_{\text{vir}}^3}{GM} \right)^{1/2}. \quad (\text{A3})$$

In more convenient units, we write the half-mass crossing time as

$$t_{\text{hm}} = 57 \left(\frac{[M_{\odot}]}{M_{\text{tot}}} \right)^{1/2} \left(\frac{r_{\text{hm}}}{[\text{pc}]} \right)^{3/2} [\text{Myr}]. \quad (\text{A4})$$

Density center The density weighted average of the positions of all stars (von Hoerner 1960, 1963):

$$\mathbf{r}_{\text{dens}}^{\text{VH}} \equiv \frac{\sum_i \mathbf{r}_i \rho_j^{(i)}}{\sum_i \rho_j^{(i)}} \quad (\text{A5})$$

In these expressions, $\rho_j^{(i)}$ is the density estimator of order j around the i -th particle, with position vector \mathbf{r}_i . For any star i we define the local density within the volume V_j of the sphere containing the j nearest neighbors (i_1, i_2, \dots, i_j) of i as

$$\rho_j^{(i)} \equiv \frac{\sum_{k=1}^{j-1} m_{i_k}}{V_j}, \quad (\text{A6})$$

where $V_j = \frac{4\pi}{3} |r_{i_j} - r_i|^3$, and the sum over masses excludes the masses of both stars i and i_j (see Casertano & Hut 1985). We take $j = 12$.

Escaper: A star which is not bound to the cluster, i.e. whose energy exceeds the energy at the cluster’s Jacobi surface. An escaper may lie within the Jacobi surface.

Half mass radius: The radius of the sphere, centered on the cluster density center, that contains half of the total cluster mass (as defined in the text). It is not always clear which stars to include in determining this radius, as the cluster is generally flattened in the Galactic tidal field.

Hard binary: A binary whose binding energy exceeds the mean stellar energy in the cluster (Heggie 1975). A binary is hard if its semi major axis exceeds

$$a = \frac{GMm(M + m + m_3)}{(M + m)m_3v^2}. \quad (\text{A7})$$

Jacobi radius: The distance from the cluster center to the L_1 and L_2 Lagrange points—the maximum distance from the cluster center to the cluster Jacobi surface.

Jacobi surface: The cluster’s “Roche lobe” in the tidal field of the Galaxy. Consider a star moving with Jacobi integral $E_J \equiv \frac{1}{2}v^2 + \phi_{\text{eff}}(\mathbf{r})$ in the rotating frame of reference in which our simulations are performed, where v is velocity and the effective potential ϕ_{eff} includes the cluster’s self-gravity, the tidal field of the Galaxy, and the centrifugal force in the rotating frame. The *zero-velocity surface* for that value of E_J is defined by $v = 0$, so $\phi_{\text{eff}}(\mathbf{r}) = E_J$ (Binney & Tremaine 1987). The Jacobi surface for the cluster is defined to be the last closed zero-velocity surface that contains the cluster—that is, the surface passing through the cluster’s L_1 and L_2 Lagrange points. With the conventions adopted in *kira*, the Lagrange points are located along the x -axis, the cluster orbits in the x - y plane, and the Jacobi surface is elongated in the x -direction. The three coordinate axes intersect the Jacobi surface at distances $r_x = r_J$ (the Jacobi radius), r_y , and r_z from the cluster center.

Member: A star (or multiple system) which is bound to the cluster. The energy of such a star is less than the energy at the cluster Jacobi surface. A member may lie outside the Jacobi surface.

Primary: The more massive of the two stars in a binary system. Denoted with M .

Relaxation time: We use Spitzer’s (1987) definition of the half mass relaxation time:

$$t_{\text{rlx}} = \left(\frac{r_{\text{hm}}^3}{GM} \right)^{1/2} \frac{N}{8 \log \Lambda}. \quad (\text{A8})$$

Here $\Lambda \simeq 0.4N$ is the Coulomb logarithm. (In the presence of a realistic mass function, $\Lambda \lesssim 0.1N$ may be more appropriate; Farouki & Salpeter 1982; 1994; Smith, 1992; Fukushige & Heggie 1999). In convenient units this may be written

$$t_{\text{rlx}} = 2.05 \left(\frac{[M_\odot]}{M_{\text{tot}}} \right)^{1/2} \left(\frac{r_{\text{hm}}}{[\text{pc}]} \right)^{3/2} \frac{N}{\log \Lambda} [\text{Myr}]. \quad (\text{A9})$$

Note that “ N ” here is the number of bound objects in the star cluster, and is smaller than the total number of stars if the cluster contains binaries.

Secondary: The less massive of the two stars in a binary system. Denoted with m .

Tidal radius: Since clusters are somewhat elongated in the Galactic tidal field, the tidal “radius” is not well defined. For definiteness, we take the tidal radius to be the Jacobi radius of the cluster. For a disk field described by Oort (1927) constants A and B , we have

$$r_{\text{tide}}^3 = \frac{GM_{\text{tot}}}{4A(A - B)} [\text{pc}]. \quad (\text{A10})$$

In the solar neighborhood, $A = 15 \text{ km s}^{-1} \text{ kpc}^{-1}$, and $B = -12 \text{ km s}^{-1} \text{ kpc}^{-1}$.

Unperturbed binary: A binary for which the dimensionless perturbation due to its neighbors is less than some critical value ($\sim 10^{-6}$, typically). Dynamically, unperturbed binaries are treated in the point-mass approximation, as seen by the rest of the system. Only unperturbed binaries can be treated using the *SeBa* binary evolution module described in Appendix B. Perturbed binaries are treated as two single stars; mass transfer and tidal circularization are currently not handled in perturbed binaries.

Virial radius: A characteristic length scale for the system, defined by

$$r_{\text{vir}} = \frac{GM_{\text{tot}}^2}{-2U}, \quad (\text{A11})$$

where M_U is the total potential energy of the system (including the tidal potential). For an isolated equal-mass system, r_{vir} is the harmonic mean of the particle separations (Hénon 1972).

APPENDIX B: STARLAB

The simulations described in this series of papers are carried out within the “Starlab” software environment, version 3.5. Starlab is a software package for simulating the evolution of dense stellar systems and analyzing the resultant data. It consists of a collection of loosely coupled programs (“tools”) linked at the level of the UNIX operating system. The tools share a common data structure and can be combined in arbitrarily complex ways to study the dynamics of star clusters and galactic nuclei. The main components of Starlab used in this work are *kira*, the N -body integrator, and *SeBa*, a stellar and binary evolution package. The Starlab system is described in detail in <http://www.sns.ias.edu/~starlab>.

B1 Kira

The N -body integrator *kira* is the largest single program within Starlab. Its basic function is to take an input N -body system and evolve it forward for a specified period of time, producing snapshot and other diagnostic output at regular intervals. In addition to strictly dynamical evolution of stars and multiple stellar systems, *kira* also incorporates stellar and binary evolution (via the *SeBa* subpackage), and the possible influence of an external (“tidal”) gravitational field. The program is designed to take advantage of the “GRAPE-4” special-purpose processor (Makino et al. 1997), if available, although GRAPE is not required for its operation.

B1.1 The Integrator

Particle motion is followed using a fourth-order, block-timestep (McMillan 1986) “Hermite” predictor-corrector scheme (Makino and Aarseth 1992). Briefly, during a time step δt , particle positions \mathbf{x} and velocities \mathbf{v} are first predicted using the known acceleration \mathbf{a} and “jerk” \mathbf{j} (the time derivative of the acceleration):

$$\mathbf{x}_p = \mathbf{x} + \mathbf{v}\delta t + \frac{1}{2}\mathbf{a}\delta t^2 + \frac{1}{6}\mathbf{j}\delta t^3, \quad (\text{B1})$$

$$\mathbf{v}_p = \mathbf{v} + \mathbf{a}\delta t + \frac{1}{2}\mathbf{j}\delta t^2. \quad (\text{B2})$$

The acceleration \mathbf{a}_p and jerk \mathbf{j}_p are then computed at the predicted time using \mathbf{x}_p and \mathbf{v}_p , and the motion is corrected using the additional derivative information thereby obtained,

$$\mathbf{k} \equiv \frac{1}{2}\mathbf{a}''\delta t^2 = 2(\mathbf{a} - \mathbf{a}_p) + \delta t(\mathbf{j} - \mathbf{j}_p), \quad (\text{B3})$$

$$\mathbf{l} \equiv \frac{1}{6}\mathbf{a}''' \delta t^3 = -3(\mathbf{a} - \mathbf{a}_p) - \delta t(2\mathbf{j} + \mathbf{j}_p), \quad (\text{B4})$$

to obtain the corrected position and velocity:

$$\mathbf{x}_c = \mathbf{x}_p + \left(\frac{1}{20}\mathbf{l} + \frac{1}{12}\mathbf{k}\right)\delta t^2, \quad (\text{B5})$$

$$\mathbf{v}_c = \mathbf{v}_p + \left(\frac{1}{4}\mathbf{l} + \frac{1}{3}\mathbf{k}\right)\delta t. \quad (\text{B6})$$

A single integration step in thus proceeds as follows:

(i) Determine which stars are to be updated next. Each star has associated with it an individual time t , representing the time to which it was last advanced, and an individual

timestep δt . The list of stars to be integrated consists of those with the least value of $t + \delta t$. Time steps are constrained to be powers of 2, allowing “blocks” of many stars to be advanced simultaneously.

(ii) Before the step is actually taken, check for

- (a) termination of the run
- (b) escaper removal
- (c) system reinitialization
- (d) diagnostic (“log”) output, which includes
 - information on bulk parameters of the system: total mass, energy, momentum, anisotropy, etc.
 - technical information on CPU time, timestep distribution, etc.
 - detailed information on the cluster mass distribution: core properties, Lagrangian radii, etc.
 - stellar mass distribution and anisotropy by Lagrangian zone
 - luminosity profile, and mass and luminosity functions
 - cluster stellar content (by spectral type and luminosity class)
 - detailed dynamical and physical data on all binary systems.

(e) snapshot output, for restart and display

(iii) Perform low-order prediction of all particles to the new time. This operation may be performed on the GRAPE, if present.

(iv) Recompute the acceleration and jerk on all stars in the current block (using the GRAPE, if available), and correct their positions and velocities for fourth-order accuracy.

(v) Check for and initiate unperturbed motion.

(vi) Check for collisions and mergers.

(vii) Check for tree reorganization (see below).

(viii) Check for and apply stellar and/or binary evolution (§B.2), and correct the dynamics as necessary.

B1.2 Tree Structure

An N -body system in Starlab is represented as a linked-list structure, in the form of a mainly “flat” tree having individual stars as leaves. The tree is flat in the sense that single stars (i.e. stars that are not members of any multiple system) are all represented as top-level nodes, having the root node (the system center of mass) as parent. Binary, triple, and more complex multiple systems are represented as binary trees below their top-level center of mass nodes. The tree structure determines both how node dynamics is implemented and how the long-range gravitational force is computed.

Each parent node contains “local” information about its dynamics—mass, position, velocity, etc.—relative to its parent node. The leaves contain additional information about

stellar properties—effective radius, luminosity, temperature, etc. The parent node of a unperturbed binary also contains information on the binary parameters—semi-major axis, eccentricity, mean anomaly, etc. The motion of every node *relative to its parent node* is followed using the Hermite predictor-corrector scheme just described. The use of relative coordinates at every level ensures that high numerical precision is maintained at all times, even during very close encounters.

The tree evolves dynamically according to simple heuristic rules: particles that approach “too close” to one another are combined into a center of mass and binary node; and when a node becomes “too large” it is split into its binary components. These rules apply at all levels of the tree structure, allowing arbitrarily complex systems to be followed. In practice, the term “too close” is taken to mean that two stars (1 and 2) approach within the “close-encounter distance” $R_{\text{close}} \sim r_{\text{vir}}(m_1 + m_2)/2M_{\text{tot}}$, the impact parameter that would lead to a 90° deflection if both bodies moved at typical stellar speeds. “Too large” means that a node’s diameter exceeds $2.5R_{\text{close}}$.

B1.3 Binaries

How the acceleration (and jerk) on a particle or node is computed depends on its location in the tree. Top-level nodes feel the force due to all other top-level nodes in the system. Forces are computed using direct summation over all other particles in the system; no tree or neighbor-list constructs are used. (This procedure is designed specifically to allow efficient computation of these forces using GRAPE hardware, if available.) Nearby binary and multiple systems are resolved into their components, as necessary.

The internal motion of a binary component is naturally decomposed into two parts: (1) the dominant contribution due to its companion, and (2) the perturbative influence of the rest of the system. This decomposition is applied recursively, at all levels in a multiple system. Since the perturbation drops off rapidly with distance from the binary center of mass, usually only a few near neighbors are significant perturbers of even a moderately hard binary. These neighbors are most efficiently handled by maintaining lists of perturbers for each binary. Perturber lists are recomputed at time the center of mass is integrated.

A further efficiency measure is the imposition of *unperturbed motion* for binaries whose perturbation falls below some specified value for all or part of an orbit. Unperturbed binaries may be followed analytically for many orbits as strictly two-body motion; they are also treated as point masses, from the point of view of their influence on other stars. The use of the unperturbed approximation near the periastron of eccentric orbits was a key element in our decision not to use cumbersome regularization schemes for the computation of binary motion.

Because unperturbed binaries are followed in steps that are integer multiples of the orbit period, we can relax the

perturbation threshold for unperturbed motion relative to that for a perturbed step (since most of the perturbative effects of nearby stars are periodic). Perturbed binaries are resolved into their components, both for purposes of determining their center of mass motion and for determining their effect on other stars. Unperturbed treatments of multiple systems are also used, based on empirical studies of the stability of their internal motion. A hierarchical system is regarded as stable if (a) the external perturbation is less than some threshold value, and (b) each component is stable (or single), by the same criterion.

“Lightly perturbed” binaries, having external perturbations within a factor of ~ 10 of the unperturbed threshold, are treated using a variant of the method described by Mikkola & Aarseth (1998), in which the internal motion of the binary is artificially slowed and the perturbation is increased by the same factor. Briefly, the result is that long-term secular trends in the binary orbital elements are properly reproduced, while periodic perturbative terms are amplified; the latter effect is suppressed by following the “slow” motion over an integral number of orbits. Our “slow” binary treatment differs from that of Aarseth mainly in that it is not coupled to a regularization scheme—it is applied directly to the unregularized equations of motion. In addition, we apply pairwise corrections to forces between perturbers and the binary center of mass in order to avoid spurious high derivatives caused by the mismatch between the (slowed) internal motion and the (normal) external interaction.

B1.4 Tidal Field

The standard form of the external (tidal) potential is

$$\phi_{\text{ext}} = \frac{1}{2}(\alpha_1 x^2 + \alpha_3 z^2). \quad (\text{B7})$$

This expression includes contributions from both the Galactic tidal field and the centrifugal force in the cluster’s rotating frame of reference. The Galactic center is assumed to lie along the negative x axis and the rotation vector $\boldsymbol{\Omega}$ is in the z direction. (We assume motion in a circular orbit in the x – y plane around the Galactic center.) The equations of motion also include a Coriolis acceleration $\mathbf{a}_c = -2\boldsymbol{\Omega} \times \mathbf{v}$. Tidal and coriolis effects are applied to top-level nodes only—that is, we neglect the tidal effect of the Galaxy on a binary’s internal motion.

The values of α_1 , α_3 , and Ω depend on the details of the field being modeled. Some common examples are:

(i) *Point-mass field.* If the Galaxy is represented as a point mass M_G at distance R_G , we have

$$\alpha_3 = -\frac{1}{3}\alpha_1 = \Omega^2 = \frac{GM_G}{R_G^3}. \quad (\text{B8})$$

(ii) *Isothermal field.* For motion in a “halo” mass distribution modeled as an isothermal sphere ($\rho \sim r^{-2}$), with $M(< r) = M_G(r/R_G)$, we have

$$\alpha_3 = -\frac{1}{2}\alpha_1 = \Omega^2 = \frac{GM_G}{R_G^3}. \quad (\text{B9})$$

(iii) *Disk field.* For motion in a disk described by local Oort constants A and B , with local density ρ_D , we have

$$\alpha_1 = -4A(A - B) \quad (\text{B10})$$

$$\alpha_3 = 4\pi G\rho_D + 2(A^2 - B^2) \quad (\text{B11})$$

$$\Omega = A - B \quad (\text{B12})$$

In the (fairly good) approximation that the gravitational potential of the cluster stars may be represented close to the Jacobi surface simply as $\phi_C(r) \sim -GM_{\text{tot}}/r$, where M_{tot} is the cluster mass, the Jacobi radius may straightforwardly be shown to be

$$r_J \approx \left(\frac{-GM_{\text{tot}}}{\alpha_1} \right)^{-1/3}. \quad (\text{B13})$$

The ratio α_3/α_1 determines the shape of the Jacobi surface.

B1.5 Escaper Removal

Stars are removed (“stripped”) from the system when they exceed a specified distance from the cluster center of mass (or density center). For systems without an imposed Galactic tidal field, this stripping radius is arbitrary. For systems with a tidal field, the stripping radius is usually tied to the Jacobi radius of the cluster. For the runs described in this paper, stars were stripped when their distance from the cluster center exceeded twice the instantaneous Jacobi radius.

B2 SeBa

The stellar and binary evolution package **SeBa**^{||} is fully integrated into the *kira* integrator, although it can also be used as a stand-alone module for non-dynamical applications.

B2.1 Evolution of a single star

Stars are evolved via the time dependent mass-radius relations for solar metallicities given by Eggleton et al. (1989, with corrections by Eggleton et al. 1990 and Tout et al. 1997)^{**}. These equations give the radius of a star as a function of time and the star’s initial mass (on the zero-age main-sequence—ZAMS). Neither the mass of the stellar core nor the rate of mass loss via a stellar wind are specified in this prescription. However, both quantities are important, both to binary evolution and to cluster dynamics. We include them using the prescriptions of Portegies Zwart & Verbunt (1996).

Stars are subdivided within **SeBa** into the following types:

^{||} The name **SeBa** is taken from the ancient Egyptian word for ‘to teach’, ‘the door to knowledge’ or ‘(multiple) star’. The exact meaning depends on the hieroglyphic spelling.

^{**} New equations which include metallicity dependence have recently been made available by Hurley et al. (2000), and will be implemented in the next version of **SeBa**.

planet	Various types, such as gas giants, etc.; also includes moons.
brown dwarf	Star with mass below the hydrogen-burning limit.
main sequence	Core hydrogen burning star.
Wolf-Rayet	Massive ($m > 25 M_\odot$) star which has lost its hydrogen envelope via a stellar wind.
helium star	Helium core of a stripped giant, the result of mass transfer in a binary. Subdivided into helium core, carbon core and helium giant.
subgiant	Hydrogen shell burning star.
horizontal branch	Helium core burning star.
supergiant	Double shell burning star.
Thorne-Zytkow	Shell burning hydrogen envelope with neutron star core.
black hole	Star with radius smaller than the event horizon. The result of evolution of massive ($m > 25 M_\odot$) star or collapsed neutron star.
neutron star	Subdivided into radio pulsar, X-ray pulsar and inert neutron star ($m < 2 M_\odot$).
white dwarf	Subdivided into helium dwarf, carbon dwarf and oxygen dwarf.
disintegrated	Result of Carbon detonation to Type Ia supernova.

Stellar-wind mass loss is neglected for main-sequence stars with $m < 25 M_\odot$. Following Langer (1998), more massive stars lose mass with $\dot{m} \propto m^{2.5}$ before becoming a Wolf-Rayet star (see Portegies Zwart et al. 1999, for the implementation). These stars eventually collapse into black holes with mass $m_{\text{bh}} = 0.35m_0 - 12 M_\odot$, where m_0 is the initial mass of the star. (For a star whose mass increases due to collisions or other processes, m_0 is the highest mass reached by the star. The black hole radius equals the Schwarzschild radius: $r = 2Gm/c^2$.)

A star with a helium core mass between 2.2 and 5 M_\odot becomes a neutron star. (These limits correspond to 8 M_\odot and 25 M_\odot ZAMS mass stars which evolve as isolated single stars.) At birth, a neutron star receives a velocity “kick” in a random direction. The magnitude of the velocity kick is chosen randomly from the distribution proposed by Hartman (1997)

$$P(u)du = \frac{4}{\pi} \frac{du}{(1+u^2)^2}, \quad (\text{B14})$$

with $u = v/\sigma$ and $\sigma = 600 \text{ km s}^{-1}$.

A star with a core mass less than 2.2 M_\odot sheds its envelope at the end of its evolution and becomes a white dwarf. The mass of the white dwarf equals the core mass of its progenitor at the tip of the asymptotic giant branch.

B2.2 Schematic evolution of a binary

The evolution of a single isolated or unperturbed binary is carried out in the following steps (see sects. B2.3 and B2.4 for details):

The evolution of any binary stars by Determining the binary evolution timestep. This is the smallest timestep allowed by either of the stars. A stellar evolution timestep is 1% of the time taken for the star to evolve from the start of one evolutionary stage to the next—for example, from the zero-age main sequence to the terminal-age main sequence. (The stellar evolution step is not to exceed 1Gyear.) A list of these mile-posts along a star's evolutionary is provided in Sect. B2.1. A binary is evolved whenever one of its stars requires an update.

If a binary is in a state of mass transfer (but not in a common envelope) the timestep is reduced such that < 1% of the donor' envelope is lost per step.

1. Apply angular momentum loss by magnetic stellar wind.
2. Apply angular momentum loss by gravitational wave radiation.
3. Check for coalescence.
4. Evolve primary star.
 - (a) adjust binary parameters for stellar wind mass loss
 - (b) resolve supernova.
5. Check if binary still exists. The evolution of the primary (or secondary) star may have resulted in a supernova which may disrupt the binary or resulted in a collision between the two stars.
6. Evolve secondary star.
 - (a) Adjust binary parameters for stellar wind mass loss.
 - (b) Resolve supernova.
7. Check if binary still exists (see [5.]).
8. Check for tidal circularization and synchronization.
9. Check if any star is Roche-lobe filling and identify the donor and the accretor. If no star is filling its Roche-lobe leave binary evolution and notify dynamics, otherwise proceed with the following steps
 - (a) Find moment mass transfer starts.
 - (b) Check for binary stability
 - if binary unstable apply commone envelope
 - if components merge leave binary evolution and notify dynamics.
 - (c) Calculate ζ_{ad} , ζ_{R1} and ζ_{th} .
 - (d) Determine amount of mass loss from donor.
 - (e) Determine amount of mass gained by accretor.
 - (f) Subtrac mass from donor.
 - (g) Add mass to accretor. Calculate new evolutionary state of accretor and Rejuvenate.
 - (h) Calculate new binary parameters.

B2.3 Evolution of binary parameters without mass transfer

The orbital parameters of a binary are affected by the evolution of its components. We will not present here all the many details of binary evolution, but for clarity we summarize those which affect the dynamics or are important for interpreting our results. The details of the binary evolution program **SeBa** are discussed in more detail by Portegies Zwart & Verbunt (1996) and Portegies Zwart & Yungelson (1998).

Mass lost in a stellar wind is assumed to escape isotropically from the binary system. If the companion accretes a fraction ξ of the other star's wind this implies

$$\frac{a}{a_0} = f \frac{M_0 + m_0}{M + m}, \quad (B15)$$

Here M_0 and m_0 are the initial primary and secondary mass, respectively, M and m are their final masses. And

$$f = \left(\left[\frac{M}{M_0} \right]^\xi \frac{m}{m_0} \right)^{-2}. \quad (B16)$$

The fraction ξ is calculated via Bondi–Hoyle (1944) accretion assuming that the thermal velocity in the wind equals the escape velocity of the mass-losing star (for details see Portegies Zwart & Verbunt 1996).

When the radius of one of the stars exceeds 5 times the orbital periastron separation $a(1 - e)$, orbital energy is transformed into oscillatory modes in the two stars. This leads to a decrease in the orbital separation and, due to conservation of angular momentum [$a(1 - e^2) = \text{constant}$], to the eventual circularization of the binary.

Mass loss in a supernova is lost impulsively from the binary system. As a result both the orbital separation and the eccentricity change: both increase if the pre-supernova orbit was circular. The velocity kick (Eq. B14) received by the neutron star at formation is added randomly to its orbital velocity. New orbital parameters are then calculated assuming that the positions of the two stars are unchanged, mass is lost isotropically from the exploding star, and the companion is unaffected by the explosion. If the pre-supernova orbit is eccentric things get somewhat more complicated (see Portegies Zwart & Verbunt 1996).

Low-mass stars may have magnetically coupled winds, and relatively large changes in angular momentum may occur even though a negligible amount of mass escapes. We follow the prescription described by Rappaport et al. (1983) for tidally synchronized binaries in which at least one component is a main-sequence star or (sub)giant with mass $0.7 \leq m/M_\odot \leq 1.5$.

Compact stars in short-period binaries and highly eccentric binaries lose orbital energy and angular momentum via gravitational radiation. For such binaries, we use the expressions provided by Peters (1964) to compute the time dependence of the orbital semi-major axis and eccentricity.

B2.4 Mass transfer in binaries

When one star in a binary approaches its Roche-limit, we iteratively determine the moment at which contact occurs. The size of the Roche lobe is calculated as (Eggleton 1983)

$$r_{\text{Rl}} = \frac{0.49}{0.6 + q^{2/3} \ln(1 + q^{-1/3})}, \quad (\text{B17})$$

where $q \equiv m/M$. The Roche-lobe-filling star is then identified as the donor and its companion as the accretor.

B2.4.1. Unstable Mass transfer

When a star fills its Roche lobe we first check for the possibility of Darwin-Riemann instability. This happens if

$$J_{\text{donor}} > \frac{1}{3} J_{\text{bin}}, \quad (\text{B18})$$

where J_{donor} and J_{bin} are the angular momenta of the Roche-lobe-filling star and the binary, respectively.

During spiral-in the envelope of the donor is expelled, at the cost of orbital energy, following the prescription of Webbink (1984):

$$\frac{a}{a_0} = \frac{M_c}{M} \left(\frac{1 + 2a_0}{\alpha \lambda} \frac{M_c}{m} \right)^{-1}. \quad (\text{B19})$$

The parameters governing binary evolution are listed in Table B2.

If the Roche-lobe-filling star is a main-sequence star or compact object, the two stars simply merge because the donor has no core-halo structure. If both the donor and the accretor are (sub)giants, we expel both envelopes at the cost of the binaries binding energy in a *double inspiral*. A merger occurs when the binary that remains after the common envelope phase is semi-detached, in which case no more mass is lost (see sect. B4).

B2.4.2. Stable mass transfer

We calculate the time scale for mass transfer in a dynamically stable binary by considering the responses of the donor and the binary parameters to changes in the donor mass. For this purpose we define the logarithmic derivative

$$\zeta_i = \left(\frac{d \ln r}{d \ln m} \right)_i, \quad (\text{B20})$$

for each of the following processes:

ζ_{ad}	the change in donor radius due to adiabatic adjustment of hydrostatic equilibrium
ζ_{Rl}	the change in the size of the donor's Roche lobe
ζ_{th}	the change in donor radius as it adjusts to a new thermal equilibrium

The adopted values for ζ_{ad} are as follows: For main sequence stars with $m > 0.7 M_{\odot}$ we use $\zeta_{\text{ad}} = 4$ and half this value for lower-mass main sequence stars. For stars on the Hertzsprung gap and horizontal branch we use $\zeta_{\text{ad}} = 2.25$ and 15, respectively. For other stars with a core-halo structure (subgiants, supergiants and T \ddot{Z} objects), we use the following fit to the composite polytropic models of Hjellming & Webbink (1987):

$$\zeta_{\text{ad}} = -0.221 - 2.847x + 32.03x^2 - 75.69x^4 + 57.81x^5, \quad (\text{B21})$$

where $x = m_{\text{core}}/m$.

We use ζ_{th} between 0 and 0.9 for main sequence stars and $\zeta_{\text{th}} = 0$ for all other stars, except those on the Hertzsprung gap and on the horizontal branch for which we use $\zeta_{\text{th}} = -2$ and 15, respectively.

The response of the Roche lobe to mass transfer ζ_{Rl} is calculated by transferring an infinitesimal amount of mass from the donor to the accreting star and study the response of the binary parameters. This test particle is transferred on the same timescale as was used in the previous mass transfer step. At first Roche-lobe contact, when there was no previous mass transfer step, we assume that the test particle is transferred on a thermal timescale, which is a rather conservative choice.

The time scale on which mass transfer proceeds is determined as follows:

$\zeta_{\text{ad}} < \zeta_{\text{Rl}}$	dynamically unstable mass transfer proceeds on time scale τ_{dyn}
$\zeta_{\text{ad}} > \zeta_{\text{Rl}}$ and $\zeta_{\text{th}} < \zeta_{\text{Rl}}$	thermally unstable mass transfer proceeds on time scale τ_{th}
$\zeta_{\text{ad}} > \zeta_{\text{Rl}}$ and $\zeta_{\text{th}} \geq \zeta_{\text{Rl}}$	nuclear unstable mass transfer proceeds on time scale $\min(\tau_{\text{nuc}}, \tau_{\text{J}})$,

where the time scales associated with the various criteria are as follows:

dynamic:	$\tau_{\text{dyn}} \simeq 5.1 \cdot 10^{-11} \sqrt{r^3/m}$ [Myr]
thermal:	$\tau_{\text{th}} \simeq 32m^2/(rL)$ [Myr]
nuclear:	$\tau_{\text{nuc}} \simeq 0.1 t_{\text{ms}}$
angular momentum loss:	$\tau_{\text{J}} \simeq J_{\text{bin}}/(\dot{J}_{\text{gr}} + \dot{J}_{\text{mb}})$.

Here t_{ms} is a star's main-sequence lifetime, and m , r and L are its mass, radius and luminosity, respectively. The loss of angular momentum via gravitational radiation and magnetic braking are denoted by \dot{J}_{gr} and \dot{J}_{mb} , respectively.

Table B1 gives a flavor of the various time scales on which mass transfer generally proceeds. However, the details depend critically on the orbital separation and on the mass and evolutionary state of both the donor and the accreting star.

Some mass may be lost from the binary system during mass transfer. The new orbital parameters are calculated assuming that the mass lost from the binary carries specific angular momentum η_{J} (see Table B2). We calculate the final orbital separation using

$$\frac{a}{a_0} = \left(\frac{Mm}{M_0 m_0} \right)^{-2} \left(\frac{M+m}{M_0+m_0} \right)^{2\eta_{\text{J}}+1}. \quad (\text{B22})$$

Here $M = M_0 - dM$ and $m = m_0 + dm$ (so dM and dm are defined as positive quantities). The binary thus loses mass if $dM - dm \geq 0$. For the amount of mass accepted by the accretor, see Portegies Zwart & Verbunt (1996).

Table B1. Schematic diagram of the time scales on which stable mass transfer (donor to accretor) proceeds.

<i>Donor:</i>	main sequence	subgiant	supergiant	compact object
<i>Accretor:</i>				
main sequence	nuclear/thermal	thermal	dynamic	—
(sub)giant	—	nuclear/thermal	thermal/dynamic	—
compact object	thermal/aml	dynamic	dynamic	aml

B3 Rejuvenation of the accretor

An accreting star generally becomes more massive, which shortens its evolutionary time scale. The method described here is rather ad-hoc. We assume that a star accreting δm of mass remains in the same evolutionary state (see the list in Sect. B2.1). The age of the star with mass m is $t(m)$ and we want to know what is the age $t(m + \delta m)$ of the star with mass $m + \delta m$. At the moment the mass of the accretor increases from m to $m + \delta m$ the star is in evolutionary state i . It took the star $t_i(m)$ to reach that evolutionary state and this state lasts for $\tau_i(m) \equiv t_{i+1}(m) - t_i(m)$ for a star with mass m . The same stage for a star with mass $m + \delta m$ lasts for $\tau_i(m + \delta m)$. The age of the star after accretion then becomes

$$t(m + \delta m) = t_i(m + \delta m) + \left(\frac{t(m) - t_i(m)}{\tau_i(m)} \right) \tau_i(m + \delta m) \mathcal{R}. \quad (\text{B23})$$

Here \mathcal{R} is a fraction introduced to mimick the rejuvenation of the accretor ($\mathcal{R} > 1$). The mass dumped on its surface may lead to some internal mixing, refreshing some of the helium core material with some of the freshly accreted Hydrogen. This rejuvenation fraction is calculated with

$$\mathcal{R} = \left(\frac{m + \delta m}{m} \right)^\kappa, \quad (\text{B24})$$

and we use $\mathcal{R} = 1$ if the accreted material is not Hydrogen, in which case the accretor is not rejuvenated. Allowing $\mathcal{R} < 1$ would mimick that a star becomes older upon accreting material. The adopted value for κ is listed in Table B2.

We will give two examples of a $m = 2 M_\odot$ star which accretes $\delta m = 0.2 M_\odot$ from a Helium rich companion ($\mathcal{R} = 1$). For simplicity we assume here that this amount of mass is transferred in an infinitesimal timestep. The main-sequence lifetime for a $2 M_\odot$ star is about 801 Myear and about 608 Myear for a $2.2 M_\odot$ star. If mass transfer starts at $t = 700$ Myear, the $2 M_\odot$ accretor is still on the main sequence. After mass transfer the accreting star has an age of 531 Myear and is still on the main sequence.

If mass transfer started at $t = 1$ Gyear things become somewhat more complicated. The $2 M_\odot$ accretor is then on the horizontal branch. The time it takes from zero-age to the beginning of the horizontal branch is about 938 Myear, for a $2.2 M_\odot$ star this is about 712 Myear. The $2 M_\odot$ star spends roughly 84 Myear on the horizontal branch, where a $2.2 M_\odot$ star spends only 82 Myear in that stage. Substitution of these numbers into Eq. B23 results in an age of the post mass transfer star of 773 Myear.

Table B2. Free parameters in binary evolution

term	value	description
κ	1	accretor rejuvenation factor
η_J	2	specific angular momentum loss per unit mass
λ	0.5	envelope binding energy fraction
α_{ce}	4	common envelope constant

B4 Result of a merger or collision

We have adopted a set of simple prescriptions to specify the outcome of stellar collisions. In the future these prescriptions can be refined when more accurate calculations become available. As a rule of the thumb, the result of a collision is the conservative accretion of the lower-mass star onto the more massive star. The accretor will then be rejuvenated as described in Eq. B24. This rule is violated when one component is a giant or a compact object. A detailed prescription of how to calculate the evolutionary state of such a merger is presented in paper I.

We describe our treatment of the possible outcomes of encounters between two stars, ordered by the evolutionary state of the more massive of the two (the primary). Table B3 summarizes this treatment.

B4.1 Main-sequence primary

If both stars involved in the encounter are main-sequence stars, then the less massive star is accreted conservatively onto the more massive star. The resulting star is a rejuvenated main-sequence star (see Lai et al. 1993, Lombardi et al. 1995). The details of this procedure are described in Appendix C4 of Portegies Zwart & Verbunt (1996).

If the less massive star in the encounter has a well developed core (giant or subgiant), this core becomes the core of the merger product. The main-sequence star and the envelope of the giant are combined to form the new envelope of the merger. In general, the mass of the core is relatively small compared to the mass of the envelope, and the star is assumed to continue its evolution through the Hertzsprung gap. Note that this type of encounter can only occur when the main-sequence star is itself a collision product (e.g. a blue straggler).

When a main-sequence star encounters a less massive white dwarf, we assume that the merger product is a gi-

Table B3. Simplified representation of possible merger outcomes. The four columns correspond to the four choices given for the type of massive star (primary), while the four rows indicate the type of less massive star (secondary): main-sequence star (ms), (sub)giant (sg), white dwarf (wd) and neutron star (ns). In this table we do not distinguish between stars in the Hertzsprung gap (Hg) or on the first and second ascent on the asymptotic-giant branch (AGB).

star	primary			
	ms	sg	wd	ns
ms	ms	sg	wd +	ns +
sg	Hg	AGB	wd +	ns +
wd	sg	AGB	disc	disc
ns	TŻO	TŻO	-	-

ant whose core and envelope have the masses of the white dwarf and the main-sequence star, respectively. We then determine its evolutionary state as follows. We calculate the total time t_{agb} that a single, unperturbed star with mass equal to that of the merged star would spend on the asymptotic giant-branch, and the mass $m_{c,\text{agb}}$ of its core at the tip of the giant branch. The age of the merger product is then calculated by adding $t_{\text{agb}}m_c/m_{c,\text{agb}}$ to the age of an unperturbed star with the same mass at the bottom of the asymptotic giant branch. For example, a single, unperturbed $1.4M_{\odot}$ star leaves the main-sequence after 2.52 Gyr, spends 60 Myr in the Hertzsprung gap, moves to the horizontal branch at 2.96 Gyr, and reaches the tip of the asymptotic giant branch after 3.06 Gyr, with a core of $0.64M_{\odot}$. Thus, if a $0.6M_{\odot}$ white dwarf merges with an $0.8M_{\odot}$ main-sequence star, the merger product has an age of 2.87 Gyr, leaving it another 180 Myr before it reaches the tip of the asymptotic giant-branch.

If the less massive star is a neutron star or black hole a Thorne–Żytkow object (1977) is formed.

B4.2 Evolved primary

When a (sub)giant or asymptotic branch giant encounters a less massive main-sequence star, the main-sequence star is combined with the envelope of the giant, which stays in the same evolutionary state. Its age within that state is changed, however, according to the rejuvenation calculation described in Sect. C3 of Portegies Zwart & Verbunt (1996). For example, an encounter of a giant of $0.95M_{\odot}$ and

age 11.34 Gyr with a $0.45M_{\odot}$ main-sequence star produces a giant of $1.4M_{\odot}$ with an age of 2.67 Gyr.

When both stars are (sub)giants, the two cores are merged and form the core of the merger product (see Davies et al. 1991 and Rasio & Shapiro 1995). Half the envelope mass of the less massive star is accreted onto the primary. The merger product continues its evolution starting at the next evolutionary state—a (sub)giant continues its evolution on the horizontal branch, and a horizontal branch star becomes an asymptotic-giant branch star. The reasoning behind this assumption is that an increased core mass corresponds to a later evolutionary stage.

If the less massive star is a white dwarf, then its mass is simply added to the core mass of the giant, and the envelope is retained. If the age of the giant before the encounter exceeds the total lifetime of a single unperturbed star with the mass of the merger, then the newly formed giant immediately sheds its envelope and its core turns into a single white dwarf. Otherwise the merged giant is assumed to have the same age (in years) as the giant before the collision, and continues its evolution as a single unperturbed star.

If the other star is a less massive neutron star, a Thorne–Żytkow object is formed.

B4.3 White-dwarf primary

In an encounter between a white dwarf and a less massive main-sequence star, the latter is assumed to be completely disrupted, and forms a disk around the white dwarf (Rasio & Shapiro 1991). The white dwarf accretes from this disk at a rate of 1 percent of the Eddington limit. If the mass in the disc exceeds 5% of the mass of the white dwarf, the excess mass is expelled from the disc at a rate equal to the Eddington limit.

If a white dwarf encounters a less massive (sub)giant, a new white dwarf is formed with a mass equal to the sum of the pre-encounter core of the (sub)giant and the white dwarf. The newly formed white dwarf is surrounded by a disk formed from half the envelope of the (sub)giant before the encounter. The factor half is rather arbitrary and based on the lack of detailed calculations which provide a proper number. If the mass of the white dwarf exceeds the Chandrasekhar limit it explodes in a type Ia supernova, leaving no remnant (Nomoto & Kondo 1991; Livio & Truran 1995).

A collision between two white dwarfs results in a single white dwarf with mass equal to the sum of the original masses. If the total mass of the collision product exceeds the Chandrasekhar mass, it explodes in a type Ia supernova.

Collisions between white dwarfs and neutron stars or black holes result in the formation of an accretion disc around the compact object; the white dwarf is destroyed. Following the accretion, the neutron star may collapse into a black hole.

B4.4 Neutron-star or black-hole primary

All collisions involving a neutron star or black hole primary lead to the formation of a massive disk around the compact star. If the compact star had a disk prior to the collision, this disk is expelled. This disk accretes onto the compact star. We chose, rather arbitrarily that the accretion rate is 5% of the Eddington limit. An accreting neutron star turns into a millisecond radio pulsar, or—when its mass exceeds $2M_{\odot}$ —into a black hole.

B5 Communication between SeBa and kira

Due to the interaction between stellar evolution and stellar dynamics, it is difficult to solve for the evolution of both systems in a completely self-consistent way. The trajectories of stars are computed using a block timestep scheme, as described earlier. Stellar and binary evolution is updated at fixed intervals (every 1/64 of a crossing time, typically a few thousand years). Any feedback between the two systems may thus experience a delay of at most one timestep. Internal evolution time steps may differ for each star and binary, and depend on binary period, perturbations due to neighbors, and the evolutionary state of the star. Time steps in this treatment vary from several milliseconds up to (at most) a million years.

After each 1/64 of a crossing time, all stars and binaries are checked to determine if evolutionary updates are required. Single stars are updated every 1/100 of an evolution timestep or when the mass of the star has changed by more than 1% since the last update. A stellar evolution timestep is the time taken for the star to evolve from the start of one evolutionary stage to the next (see sect. B2.2).

After each stellar evolution step the dynamics is notified of changes in stellar radii, but changes in mass are, for reasons of efficiency, not passed back immediately (mass changes generally entail recomputing the accelerations of all stars in the system). Instead, the “dynamical” masses are modified only when the mass of any star has changed by more than 1%, or if the orbital parameters, semi-major axis, eccentricity, total mass or mass ratio of any binary has changed by more than 0.1%.

B6 Mass loss from stars and binaries

Fast (sudden) and slow (gradual) mass loss affects the dynamics of the stellar system in different ways. Mass loss is considered fast when it takes place within a fraction of an orbital time scale. For single stars, this time scale is on the order of the crossing time of the star cluster. For binaries, it is much shorter—on the order of the binary orbital period. Mass loss during a supernova explosion is considered fast, stellar winds and mass lost from a binary during mass transfer are considered slow.

Due to the discretized time steps of the stellar dynamics and the stellar evolution, from the point of view of the dynamics mass is lost in “bursts.” For example, an asymptotic

giant star with a strong stellar wind may lose its entire envelope in a hundred steps spanning roughly one crossing time, while a supergiant might lose its entire envelope instantaneously in a supernova. Mass loss for single stars affects the dynamics of the entire stellar system. For binaries and multiple systems, mass loss from a member star directly affects the orbital characteristics of its neighbors.

The rate of mass loss is particularly important for binaries. Slow mass loss via a stellar wind will soften a binary system, but will not affect its eccentricity or its center of mass velocity. (This is true if the binary is unperturbed. In a perturbed binary, the eccentricity and center of mass velocity are both affected by stellar wind mass loss.) Sudden mass loss, on the other hand, can dramatically affect the binary’s internal parameters. For unperturbed binaries, the effects of mass loss from both component stars are computed consistently using SeBa. Changes in binary parameters are calculated and the dynamics is notified, thereby transmitting the information to the rest of the stellar system via the integrator.

For perturbed binaries and multiples (and also hierarchical systems where the inner binary is unperturbed), the integrator takes care of the dynamical effects of stellar mass loss. By construction, mass transfer cannot occur in a perturbed binary or multiple system. If a supernova occurs in a perturbed binary, any slow mass loss is accounted for before fast mass loss occurs, since a star which is about to explode generally loses a significant fraction of its mass in a stellar wind before the supernova event itself. Supernova remnants do not lose mass. This assumption breaks down when the binary companion of the exploding star loses a significant fraction of its mass between the moment of the supernova and the end of the stellar update timestep. (This can happen if the binary companion is either a Wolf-Rayet star or a supergiant.) The stellar evolution time steps in these cases are taken sufficiently small (on the order of a hundred years) to ensure that this causes a negligible error.

B7 Collisions and mergers

We draw a distinction between “mergers” and “collisions.” A merger may result from mass transfer or a common-envelope phase during the evolution of an unperturbed binary. The binary node is then replaced by the merger product. The product of a merger is generally different from the result of a collision, since a merger is often preceded by a phase of mass transfer which affects the masses of both stars.

Collisions may occur between between single stars (which are part of a binary tree) or between stars in a perturbed binary. Since the integrator may miss the precise moment of closest approach, the orbital elements of each “close” pair of stars is calculated after each integration step. A collision occurs when the stars are found to be within d_{coll} times the sum of their radii at periastron: $p < d_{\text{coll}}(r_1 + r_2)$. In this case, the two stars are replaced by the collision product, which is placed in the center of mass and with the center of

mass velocity of the original two-body system. The characteristics of the collision product are calculated using **SeBa** (Sect. B4).

A collision may also occur when an unperturbed binary in a state of mass transfer is perturbed by a close encounter with another cluster member. Such a induced collision may be triggered by a close flyby, or in a multiple system with a perturbed outer orbit. The collision occurs if the sum of the component radii exceeds the distance between the two stars at the moment the binary becomes perturbed.

Acknowledgments We thank Douglas Heggie, Ken Janes, Gijs Nelemans, Koji Takahashi and Lev Yungelson for numerous discussions. This work was supported by NASA through Hubble Fellowship grant HF-01112.01-98A awarded (to SPZ) by the Space Telescope Science Institute, which is operated by the Association of Universities for Research in Astronomy, Inc., for NASA under contract NAS 5-26555, and by ATP grant NAG5-6964 (to SLWM). SPZ is grateful to Drexel University, Tokyo University and the University of Amsterdam (under Spinoza grant 0-08 to Edward P.J. van den Heuvel) for their hospitality. Special thanks goes to the University of Tokyo for providing time on their GRAPE-4 system.

REFERENCES

- Aarseth, S. J. 1973, *Vistas in Astronomy*, 15, 13
Aarseth, S. J. 1975, in *IAU Symp. 69: Dynamics of Stellar Systems*, Vol. 69, 57
Aarseth, S. J., Lecar, M. 1975, *ARAA*, 13, 1
Abt, H. A., Levy, S. G. 1972, *ApJ*, 172, 355
Andrievsky, S. . M. 1998, *A&A*, 334, 139
Anthony-Twarog, B. J. 1984, *AJ*, 89, 267
Bondi, H., Hoyle, F. 1944, *MNRAS*, 104, 273
Bouvier, J., Rigaut, F., Nadeau, D. 1997, *A&A*, 323, 139
Casertano, S., Hut, P. 1985, *ApJ*, 298, 80
Chernoff, D. F., Weinberg, M. D. 1990, *ApJ*, 351, 121
Cox, A. N. 1954, *ApJ*, 119, 188
Dachs, J., Kabus, H. 1989, *A&As*, 78, 25
Davies, M., Benz, W., Hills, J. 1991, *ApJ*, 381, 449
Duquennoy, A., Mayor, M. 1991, *A&A*, 248, 485
Eggen, O. J. 1993, *AJ*, 106, 642
Eggleton, P. P. 1983, *ApJ*, 268, 368
Eggleton, P. P., Fitchett, M. J., Tout, C. A. 1990, *ApJ*, 354, 387
Eggleton, P. P., Tout, C. A., Fitchett, M. J. 1989, *ApJ*, 347, 998
Farouki, R. T., Salpeter, E. E. 1982, *ApJ*, 253, 512
Farouki, R. T., Salpeter, E. E. 1994, *ApJ*, 427, 676
Frandsen, S., Dreyer, P., Kjeldsen, H. 1989, *A&A*, 215, 287
Fukushige, T., Heggie, D. C. 1995, *MNRAS*, 276, 206
Fukushige, T., Heggie, D. C. 1999, *MNRAS* submitted
Gatewood, G., Castelaz, M., Han, I., Persinger, T., Stein, J., Stephenson, B., Tangren, W. 1990, *ApJ*, 364, 114
Goodman, J., Hut, P. 1989, *Nat*, 339, 40
Hambly, N. C., Jameson, R. F. 1991, *MNRAS*, 249, 137
Hambly, N. C., Steele, I. A., Hawkins, M. R. S., Jameson, R. F. 1995b, *MNRAS*, 273, 505
Hambly, N. C., Steele, I. A., Hawkins, M. R. S., Jameson, R. F. 1995a, *A&As*, 109, 29
Harris, G. L. H., Fitzgerald, M. P. V., Mehta, S., Reed, B. C. 1993, *AJ*, 106, 1533
Hartman, J. W. 1997, *A&A*, 322, 127
Hartwick, F. D. A., Hesser, J. E. 1971, *PASP*, 83, 53
Hawley, S. L., Tourtellot, J. G., Reid, I. N. 1999, *AJ*, 117, 1341
Heacutenon, M. 1972, in *IAU Colloq. 10: Gravitational N-Body Problem*, p. 406
Heggie, D. C. 1975, *MNRAS*, 173, 729
Heggie, D. C. 1992, *Nat*, 359, 772
Heggie, D. C., Giersz, M., Spurzem, R., Takahashi, K. 1997, in *Highlights of Astronomy Vol. 11*. Kluwer, Dordrecht (ed. J. Andersen)
Heggie, D. C., Ramamani, N. 1995, *MNRAS*, 272, 317
Hjellming, M. S., Webbink, R. F. 1987, *ApJ*, 318, 794
Hodgkin, S. T., Pinfield, D. J., Jameson, R. F., Steele, I. A., Cossburn, M. R., Hambly, N. C. 1999, *MNRAS*, 310, 87
Hurley, J. R., Pols, O. R., Tout, C. A. 2000, submitted for publication in *MNRAS*
Hut, P., McMillan, S., Goodman, J., Mateo, M., Phinney, S., Pryor, C., Richer, H., Verbunt, F., Weinberg, M. 1992, *PASP*, 104, 981
Ianna, P. A., Adler, D. S., Faudree, E. F. 1987, *AJ*, 93, 347
Jones, B. F., Stauffer, J. R. 1991, *AJ*, 102, 1080
King, I. R. 1966, *AJ*, 71, 64
Koester, D., Reimers, D. 1981, *A&A*, 99, L8
Koester, D., Reimers, D. 1996, *A&A*, 313, 810
Kroupa, P. 1995a, *MNRAS*, 277, 1507
Kroupa, P. 1995b, *MNRAS*, 277, 1491
Kroupa, P. 1995c, *MNRAS*, 277, 1522
Lai, D., Rasio, F. A., Shapiro, S. L. 1993, *ApJL*, 406, L63
Langer, N. 1998, *A&A*, 329, 551
Livio, M., Truran, J. W. 1985, *ApJ*, 389, 695
Lombardi, J. C. J., Rasio, F. A., Shapiro, S. L. 1995, *ApJL*, 445, L117
Lynga, G. 1987, in *Catalog of open cluster data*, Computer based catalogue available through the CDS, Strasbourg, France and through NASA Data Center, Greenbelt, Maryland, USA. 5th edition, Vol. 4, p. 121
Makino, J., Aarseth, S. J. 1992, *PASJ*, 44, 141
Makino, J., Taiji, M., Ebisuzaki, T., Sugimoto, D. 1997, *ApJ*, 480, 432
McMillan, S., Hut, P. 1994, *ApJ*, 427, 793
McMillan, S., Hut, P., Makino, J. 1990, *ApJ*, 362, 522
McMillan, S., Hut, P., Makino, J. 1991a, *ApJ*, 372, 111
McMillan, S. L. W. 1986, *ApJ*, 307, 126
McMillan, S. L. W., Hut, P., Makino, J. 1991b, *Star Cluster Evolution with Primordial Binaries*, 421, *ASP Conf. Ser. 13: The Formation and Evolution of Star Clusters*
Mermilliod, J. C., Mayor, M. 1999, in 10 pages, 3 tables, 7 eps figures. Accepted for *A&A*; LaTeX Preprint no. IAUL preprint no 85., 11405
Mermilliod, J. C., Weis, E. W., Duquennoy, A., Mayor, M. 1990, *A&A*, 235, 114
Meylan, G., Heggie, D. C. 1997, *A&Ar*, 8, 1
Mikkola, S., Aarseth, S. J. 1998, *New Astronomy*, 3, 309
Nomoto, K., Kondo, Y. 1991, *ApJL*, 367, 19
Nordstroem, B., Andersen, J., Andersen, M. I. 1996, *A&As*, 118, 407
Nordstroem, B., Andersen, J., Andersen, M. I. 1997, *A&A*, 322, 460
Oort, J. 1927, *ban*, 3, 275
Oort, J. H. 1979, *A&A*, 78, 312

- Perryman, M. A. C., Brown, A. G. A., Lebreton, Y., Gomez, A., Turon, C., De Strobel, G. C., Mermilliod, J. C., Robichon, N., Kovalevsky, J., Crifo, F. 1998, *A&A*, 331, 81
- Peters, P. C. 1964, *Phys. Rev.*, 136, 1224
- Pinfield, D. J., Jameson, R. F., Hodgkin, S. T. 1998, *MNRAS*, 299, 955
- Portegies Zwart, S. F., Hut, P., Makino, J., McMillan, S. L. W. 1998, *A&A*, 337, 363
- Portegies Zwart, S. F., Hut, P., McMillan, S. L. W., Verbunt, F. 1997a, *A&A*, 328, 134
- Portegies Zwart, S. F., Hut, P., Verbunt, F. 1997b, *A&A*, 328, 130
- Portegies Zwart, S. F., Makino, J., McMillan, S. L. W., Hut, P. 1999, *A&A*, 348, 117
- Portegies Zwart, S. F., Verbunt, F. 1996, *A&A*, 309, 179
- Portegies Zwart, S. F., Yungelson, L. R. 1998, *A&A*, 332, 173
- Raboud, D., Mermilliod, J. C. 1998, *A&A*, 329, 101
- Rappaport, S., Joss, P. C., Verbunt, F. 1983, *ApJ*, 275, 713
- Rasio, F., Shapiro, S. 1991, *ApJ*, 337, 559
- Rasio, F., Shapiro, S. 1995, *ApJ*, 438, 887
- Reid, I. N., Hawley, S. L. 1999, *AJ*, 117, 343
- Rubenstein, E. P. 1997, *PASP*, 109, 933
- Ruffert, M., Müller, E. 1990, *A&A*, 238, 116
- Sandrelli, S., Bragaglia, A., Tosi, M., Marconi, G. 1999, *MNRAS*, 309, 739
- Scalo, J. M. 1986, *Fund. of Cosm. Phys.*, 11, 1
- Smith, H., J. 1992, *ApJ*, 398, 519
- Spitzer, L. 1987, *Dynamical evolution of globular clusters*, Princeton, NJ, Princeton University Press, 1987, 191 p.
- Takahashi, K., Portegies Zwart, S. F. 1998, *ApJ*, in press
- Terlevich, E. 1987, *MNRAS*, 224, 193
- Thorne, K. S., Żytkow, A. N. 1977, *ApJ*, 212, 832
- Tinsley, B. M. 1974, *PASP*, 86, 554
- Tout, C. A., Aarseth, S. J., Pols, O. R. 1997, *MNRAS*, 291, 732
- van Den Heuvel, E. P. J. 1975, *ApJl*, 196, L121
- van Leeuwen, F., Alphenaar, P., Brand, J. 1986, *A&As*, 65, 309
- Verbunt, F., Hut, P. 1987, in *IAU Symp. 125: The Origin and Evolution of Neutron Stars*, Vol. 125, 187
- von Hippel, T. 1998, *AJ*, 115, 1536
- von Hoerner, S. 1960, *Zeitschrift Astrophysics*, 50, 184
- von Hoerner, S. 1963, *Zeitschrift Astrophysics*, 57, 47
- Webbink, R. F. 1984, *ApJ*, 277, 355
- Weidemann, V. 1993, *A&A*, 275, 158
- Weidemann, V., Jordan, S., Iben, I., J., Casertano, S. 1992, *AJ*, 104, 1876

This figure "W6IIT0Myr.jpg" is available in "jpg" format from:

<http://arxiv.org/ps/astro-ph/0005248v1>

This figure "W6IIT622Myr.jpg" is available in "jpg" format from:

<http://arxiv.org/ps/astro-ph/0005248v1>

This figure "W6VT1512Myr.jpg" is available in "jpg" format from:

<http://arxiv.org/ps/astro-ph/0005248v1>